ChemComm
Chemical Communications

Accepted Manuscript

This article can be cited before page numbers have been issued, to do this please use: R. Zhang, Y. Yan, Z. Yi and D. Wang, *Chem. Commun.*, 2026, DOI: 10.1039/D6CC01805J.

ROYAL SOCIETY OF CHEMISTRY

rsc.li/chemcomm

ARTICLE ChemComm

View Article Online
DOI: 10.1039/D6CC01805J

ARTICLE

Revealing the Reaction Pathways and Interfacial Regulation Mechanisms of Urea Electro-Oxidation on Nickel-Based Catalysts

Riyi Zhang[1,2], Yong Yan[1,2]*, Zhihao Yi[3]*, Dong Wang[4]*

Received 00th January 20xx,
Accepted 00th January 20xx

DOI: 10.1039/x0xx00000x

With an equilibrium potential of 0.37 V versus RHE, much lower than that of the oxygen evolution reaction, the electrocatalytic urea oxidation reaction has been widely regarded as a promising anodic half reaction for reducing the energy consumption of hydrogen production while treating nitrogen containing wastewater. Its practical application, however, is still limited by sluggish kinetics arising from the complex six electron, six proton transfer process, even in high performance nickel based catalysts. In addition, the limited thermodynamic selectivity at nickel catalytic interfaces often prevents the complete conversion of urea into environmentally benign N_2. Instead, competing pathways and over oxidation of nitrogen containing intermediates can lead to the formation of soluble byproducts such as NO_2^- and NO_3^-. The release of these species not only weakens the remediation effect, but may also cause secondary pollution, including eutrophication.This review summarizes recent progress in nickel based UOR electrocatalysts, with emphasis on reaction pathways, *in situ* identification of active sites, and interface engineering across multiple scales. Particular attention is given to dynamic surface reconstruction under *operando* conditions and to the competition among the conventional Ni^{3+} mediated indirect mechanism, direct oxidation on high valence Ni^{4+} species, and the lattice oxygen mechanism. We also discuss how the two step pathway involving ammonia intermediates and dual site synergistic mechanisms may help relieve the linear scaling constraints associated with intermediate adsorption. On this basis, we outline a framework for catalyst regulation that includes atomic scale electronic structure tuning, mesoscopic control of internal electric fields in heterojunctions, and macroscopic microenvironment engineering, including ionic regulation and superaerophobic interfaces. Finally, by combining spatiotemporally resolved *in situ* characterization with standardized quantitative protocols, we highlight key challenges in capturing transient intermediates, resisting interference in real wastewater, and maintaining dynamic stability at ampere level current densities

[1] College of Environmental Science and Engineering, Beijing University of Technology, Beijing 100124, P. R. China
[2] State Key Laboratory of Materials Low-Carbon Recycling, Center of Excellence for Environmental Safety and Biological Effects, Department of Chemistry, College of Chemistry and Life Science, Beijing University of Technology, Beijing 100124, China
[3] State Key Laboratory of Chemistry for NBC Hazards Protection, Beijing 102205, China.
[4] Chair Materials for Electrical Engineering and Electronics, Institute of Materials Science and Engineering and Institute of Micro- and Nanotechnologies MarcoNano®, TU Ilmenau, Gustav-Kirchhoff-Str. 5, 98693 Ilmenau, Germany
Dr. Y. Yan* , Email: yong.yan@bjut.edu.cn; Dr. Z. Yi*, Email: 358032761@qq.com;
Dr. D. Wang*, Email: dong.wang@tu-ilmenau.de

Introduction

1.1 Research Background

Against the backdrop of climate change mitigation and the gradual depletion of fossil resources, the development of clean and sustainable hydrogen technologies has been widely regarded as an important route toward carbon neutrality.[1,2] Conventional electrochemical water splitting provides a feasible pathway for producing high-purity green hydrogen. However, its anodic half-reaction, the oxygen evolution reaction (OER), remains a major bottleneck because of its thermodynamic, durability, and economic limitations. In alkaline water electrolysis, the corresponding anodic OER, cathodic HER, and overall water-splitting reactions can be written as follows:[3]

Anodic reaction:

$$4OH^- \rightarrow O_2 + 2H_2O + 4e^- \quad (1)$$

Cathodic reaction:

View Article Online
DOI: 10.1039/D6CC01805J

$$4H_2O + 4e^- \rightarrow 2H_2 + 4OH^- (2)$$

Overall reaction:

$$2H_2O \rightarrow 2H_2 + O_2 (3)$$

The sluggish proton-coupled electron-transfer process involving four electrons requires a theoretical potential of 1.23 V (vs. RHE) and, in practical operation, usually an additional overpotential, which leads to high overall energy consumption. At the same time, the strongly oxidative anodic potentials required for OER tend to accelerate structural degradation and corrosion of the anode, thereby compromising long-term stability. In addition, the sole anodic product, oxygen (O_2), has limited economic value and offers little compensation for the large energy input. As a result, the combined burden of high energy consumption, insufficient electrode durability, and low-value products continues to restrict the large-scale commercial deployment of pure water electrolysis.[4-7]

To alleviate this thermodynamic energy penalty, replacing the OER with thermodynamically more favorable small-molecule oxidation reactions has become an important direction in electrocatalysis.[8,9] Among the available candidates, urea is particularly attractive. It is a common nitrogen-rich organic pollutant widely found in agricultural runoff, industrial effluents, and municipal sewage, and the direct discharge of untreated urea-containing wastewater can cause severe eutrophication and broader ecological damage.[10-12] From the perspective of electrochemical energy conversion, urea can also serve as an effective hydrogen donor, because the theoretical potential of the urea oxidation reaction (UOR) is only 0.37 V (vs. RHE).[13,14] Coupling the anodic UOR with the cathodic hydrogen evolution reaction (HER) in a urea-assisted electrolysis system can lower the cell voltage required for hydrogen production relative to overall water splitting, while simultaneously enabling the degradation and treatment of urea-containing wastewater. In alkaline media, the idealized UOR-assisted electrolysis can be commonly expressed as follows:[15]

Anodic reaction:

$$CO(NH_2)_2 + 6OH^- \rightarrow N_2 + CO_2 + 5H_2O + 6e^- (4)$$

Cathodic reaction:

$$6H_2O + 6e^- \rightarrow 3H_2 + 6OH^- (5)$$

Overall reaction:

$$CO(NH_2)_2 + H_2O \rightarrow N_2 + CO_2 + 3H_2 (6)$$

In this idealized pathway, replacing anodic oxygen evolution with the formation of nitrogen (N_2) and carbon dioxide (CO_2) can reduce the safety risks associated with gas crossover and the potentially explosive mixing of hydrogen and oxygen in conventional water electrolysis. In this sense, urea-assisted electrolysis offers a practical route that integrates wastewater treatment, improved operational safety, and energy-efficient hydrogen production.[16,17]

1.2 Predominance of Nickel-based Catalysts and Critical Bottlenecks

In the search for high-performance electrocatalysts for the UOR, noble metals such as Pt and Ru showed appreciable activity in early studies. However, under conventional alkaline UOR conditions, their apparent UOR activity and operational durability are generally less competitive than those of optimized Ni-based catalysts.[18] Their broader application is further limited by high cost and by susceptibility to deactivation arising from the strong adsorption of poisoning intermediates, such as *CO, which makes them less suitable for large-scale wastewater electrolysis.[19,20] By contrast, nickel (Ni)-based transition-metal materials are earth-abundant and cost-effective, and they exhibit high stability and intrinsic activity in alkaline media. These advantages have established them as the dominant material platform in UOR electrocatalysis.[21,22] This behavior is closely associated with the partially filled d orbitals of Ni and its flexible multivalent redox chemistry, including $Ni^{2+}/Ni^{3+}/Ni^{4+}$ transitions. Under anodic polarization, the nickel oxyhydroxide (NiOOH) phase formed *in situ* on the surface shows strong chemisorption toward urea and promotes C-N bond activation. The catalytic process is favored under the combined action of strongly alkaline media and sufficiently positive anodic potentials. Under these conditions, abundant OH^- in the electrolyte directly participates in the proton-coupled electron transfer (PCET) steps required for deep urea deprotonation. At the same time, OH^- can neutralize the released protons and thereby suppress local interfacial acidification that would otherwise hinder the generation of active phases. The alkaline environment, together with the high anodic potential, also helps maintain the dynamic interconversion of the Ni^{2+}/Ni^{3+} redox couple and stabilize high-valent dynamic NiOOH species, which are widely regarded as central to catalytic activity. These factors collectively contribute to higher intrinsic turnover frequency and improved overall urea electrooxidation performance.[23,24] As a result, a wide range of Ni-based systems, including hydroxides, oxides, chalcogenides, phosphides, metal-organic frameworks (MOFs), and their derivatives, have been extensively developed and are now regarded as benchmark materials for pushing the performance limits of the UOR.[25,26] Representative activity benchmarks of selected Ni-based UOR electrocatalysts are summarized in Table 1. Recent overviews have also summarized the principal design strategies for UOR electrocatalysts, indicating that active-phase regulation, dual-site construction, and interfacial coupling are recurrent themes in improving Ni-based catalytic performance.[27]

Despite the promise of Ni-based materials, their practical industrial deployment is still constrained by several major scientific and engineering challenges. At the fundamental level, the UOR is a kinetically sluggish six-electron, six-proton transfer process. It involves cleavage of strong C-N bonds and the sequential evolution of multiple carbon- and nitrogen-containing intermediates, such as *CO, *NH and *COO, and therefore usually requires substantial overpotentials to proceed efficiently.[28-30] In addition, intermediate adsorption in this complex reaction network is constrained by intrinsic linear scaling relations. As a result, a single active site often cannot simultaneously achieve efficient urea activation and rapid

View Article Online
DOI: 10.1039/D6CC01805J

desorption of poisoning byproducts such as CO_2.[31,32] Under high current densities and elevated anodic potentials, the UOR also competes strongly with the OER. This competition, occurring at both the substrate and active-site levels, can lower the Faradaic efficiency of the desired products and accelerate passivation of the active phase as well as dissolution of metal centers.[33,34]

Catalyst	Substrate	Electrolyte	Activity (vs. RHE)	Ref.	Year
Ni_3Se_2@$NiMoO_4$/NF	Ni foam	1.0 M KOH + 0.33 M urea	100 mA cm^{-2} @ 1.31 V	[45]	2026
Fe-NiTe/$NiSe_2$	Ni foam	1.0 M KOH + 0.33 M urea	100 mA cm^{-2} @ 1.447 V	[46]	2026
Ce-Ni-BDC@NF	Ni foam	1.0 M KOH + 0.33 M urea	100 mA cm^{-2} @ 1.408 V	[82]	2025
Ni_2N-VN/NF	Ni foam	1.0 M KOH + 0.33 M urea	1000 mA cm^{-2} @ 1.46 V	[80]	2025
NiCoP/Co_3O_4-NF	Ni foam	1.0 M KOH + 0.33 M urea	100 mA cm^{-2} @1.34 V	[89]	2025
$Ni_2Fe(CN)_6$/NF	Ni foam	1.0 M KOH + 0.33 M urea	100 mA cm^{-2} @ 1.35 V	[35]	2021
NiClO-D	Glassy carbon	1.0 M KOH + 0.33 M urea	50 mA cm^{-2} @1.386 V	[36]	2019
Ni–O–Ti	Ti foam	1.0 M KOH + 0.33 M urea	100 mA cm^{-2} @ 1.33 V	[5]	2024
CuNiCo-7.8%Mo/CF	Carbon felt	1.0 M KOH + 0.5 M urea	500 mA cm^{-2} @ 1.44 V	[86]	2025
Co,Ge–Ni oxyhydroxide	Catalyst-coated electrode	1.0 M KOH + 0.33 M urea	448.0 mA cm^{-2} @ 1.40 V	[57]	2023

Table 1 Performance of representative Ni-based electrocatalysts for the UOR

Another unresolved issue is the reaction pathway of the UOR on Ni-based interfaces. Whether the reaction proceeds through an indirect pathway coupled to the NiOOH redox cycle, a direct pathway involving direct adsorption and oxidation of the substrate, or a lattice oxygen oxidation mechanism (LOM) that includes the participation of lattice oxygen remains under active debate. This long-standing uncertainty has hindered the rational design of catalyst microstructures.[35-37] This mechanistic complexity is also consistent with recently reported Ni-based systems that do not fully conform to the conventional NiOOH-first scenario, further underscoring the need for cautious structure–mechanism correlation in UOR catalyst design.[38] As electrocatalysis research continues to advance, the field is gradually shifting from the microscopic regulation of isolated active sites toward the coordinated optimization of entire catalytic systems. As emphasized by Li *et al.*, moving from Ni sites to system synergy is becoming an important direction for the rational design of next-generation high-performance UOR catalysts. Such system-level synergy involves not only atomic-scale electronic structure modulation, but also mesoscale interfacial field effects and integration at the macroscopic device level.[39]

1.3 Scope and Objectives of This Review

To address the mechanistic controversies and performance limitations outlined above, research on UOR electrocatalysis has gradually shifted from empirical trial-and-error exploration toward atomic-level rational design. This transition has been driven by the widespread use of advanced *in situ* spectroscopic techniques, including Raman spectroscopy, infrared spectroscopy, and synchrotron-based X-ray absorption spectroscopy, together with high-precision theoretical simulations. Recent overview articles have likewise emphasized that *in situ* characterization is increasingly important for correlating catalyst reconstruction, active-site evolution, and pathway identification in the UOR.[40] These approaches have substantially improved our understanding of the dynamic structural evolution of UOR catalysts, the nature of the genuine active sites, and the complex network of reaction intermediates under realistic operating conditions.[41-43] On the basis of these mechanistic advances, it is now possible to identify authentic active species more precisely and to better understand the reaction kinetics under dynamic working conditions. This, in turn, provides a more rational basis for catalyst design. When combined with the systematic optimization of macroscopic reaction conditions, such mechanistically guided material engineering offers a feasible route toward highly robust and high-performance UOR systems.

This review provides an overview of representative advances in electrocatalytic urea oxidation at nickel-based catalytic interfaces. It begins with a critical examination of the main mechanistic debates in the UOR field, focusing on the physicochemical features of direct and indirect oxidation pathways as well as the possible involvement of lattice oxygen. It then discusses the dynamic surface reconstruction processes through which precatalysts evolve into highly active phases, together with the factors that govern their stabilization.[44-46] In the section on regulation strategies, we further summarize how multidimensional approaches can be used to overcome activity limitations and improve energy conversion efficiency. At the regulation level, representative strategies can be viewed across four closely related aspects: electronic structures: from d-band to spin states, coordination asymmetry and defect engineering, heterojunction and built-in-electric-field engineering, and multi-scale microenvironment engineering involving ionic regulation, surface wettability, and micro/nano-architecture.[43,47-49] Finally, we

discuss future challenges associated with catalyst adaptability in real wastewater environments and with the standardization of performance evaluation protocols.[50-54] Through this review, we aim to provide a clearer theoretical framework and a practical technical roadmap (Fig. 1) for the design of next-generation nickel-based UOR electrocatalysts with high activity, high selectivity, and industrially relevant durability.

View Article Online
DOI: 10.1039/D6CC01895J

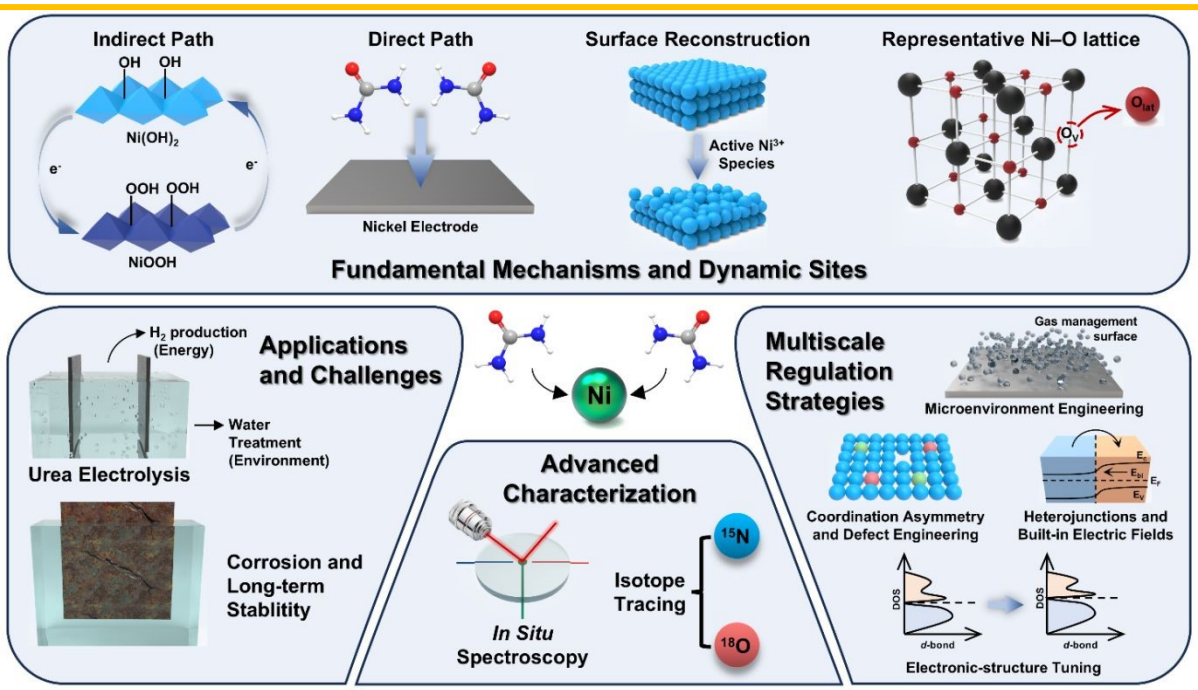

Fig. 1 Representative overview of reaction mechanisms, active-site evolution, interface-regulation strategies, advanced characterization methods, and application perspectives for the urea oxidation reaction (UOR) on nickel-based catalytic interfaces.

2. Mechanistic Insights

Despite the exceptional electrocatalytic activity exhibited by nickel-based catalysts in the alkaline urea oxidation reaction, the precise atomic-scale reaction pathways and the rate-determining step (RDS) remain subjects of intense debate due to the complexity inherent in the multi-step six-electron transfer process. High-valence NiOOH-derived Ni^{3+} species have long been regarded as central active phases; however, advances in *in situ* spectroscopy, isotope tracing, and electrochemical kinetics indicate that this picture is not universal. Direct surface oxidation on stabilized high-valent Ni sites, dual-site pathways involving local chemical conversion, and lattice-oxygen involvement may operate as alternative or complementary components, depending on the catalyst structure and operating potential.[34-36]

2.1 The Classic Mechanistic Debate: Direct Mechanism versus Indirect Mechanism

Historically, the indirect oxidation mechanism (Fig. 2a), also referred to as the catalyst regeneration mechanism, has been the dominant description for UOR on $Ni(OH)_2$/NiOOH-type electrodes in alkaline media. In this pathway, $Ni(OH)_2$ is first electrochemically oxidized to NiOOH under anodic potentials. The generated NiOOH then oxidizes urea through a chemical step and is reduced back to $Ni(OH)_2$, thereby completing the catalytic cycle, which is characteristic of an EC' mechanism. However, this electrochemical-chemical cyclic model does not fully explain the behavior of some recently reported high-activity materials, which has prompted increasing interest in the possibility of a direct mechanism (Fig. 2b). These two pathways are better regarded as limiting descriptions rather than strictly exclusive options. On a single Ni-based catalyst, direct and indirect components may coexist, and their relative contributions can change with the applied potential, surface reconstruction state, and stability of high-valent Ni species. Thus, the key issue is often which pathway dominates under a given set of operating conditions.[55]

View Article Online
DOI: 10.1039/D6CC01805J

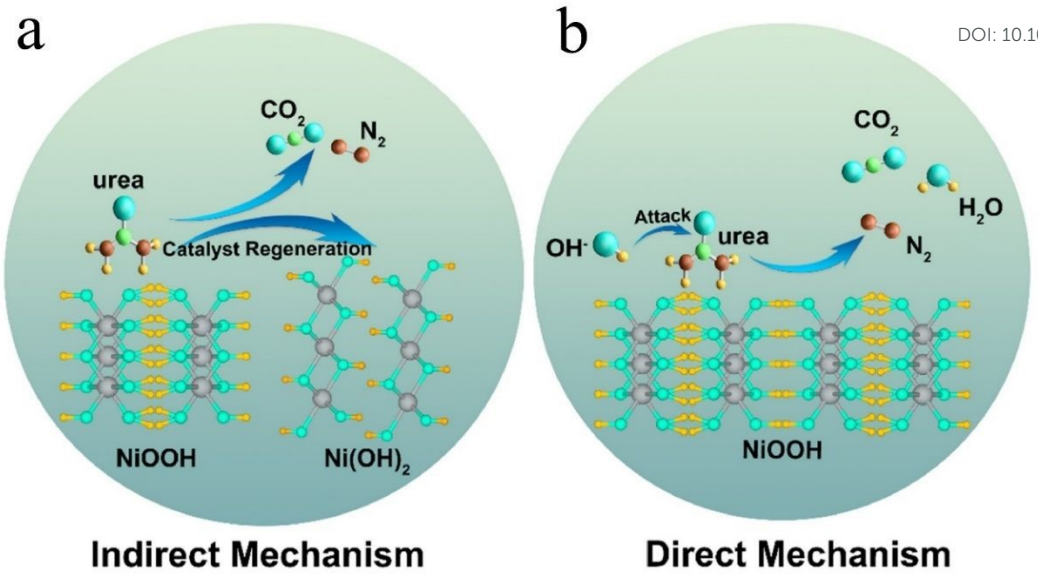

Fig. 2 Schematic illustrations of (a) the indirect reaction mechanism and (b) the direct electro-oxidation mechanism. Reproduced from ref. 101 with permission from Elsevier, Surf. Interfaces, 2023, 41, 103230, copyright 2023.

Rao et al. used a model rare-earth nickelate ($NdNiO_3$) catalyst to examine this distinction. Compared with NiO, $NdNiO_3$ retained most of the cathodic charge associated with Ni^{3+} reduction after urea was introduced, maintained a relatively high average Ni oxidation state under UOR conditions in *in situ* XANES measurements, and showed EIS features in which the high-frequency response associated with Ni^{2+}/Ni^{3+} interconversion was largely suppressed. Taken together, these observations are more consistent with a predominantly direct oxidation pathway on stabilized NiOOH species than with a conventional EC' cycle. Nevertheless, the steady-state retention of NiOOH alone does not completely exclude a fast formation–consumption equilibrium of NiOOH; direct-mechanism assignments are therefore more convincing when NiOOH retention is supported by complementary kinetic, spectroscopic, and impedance evidence.[34] To further overcome the thermodynamic limitation associated with NiOOH formation, Hou *et al.* introduced carbon-based oxyacid anions ($-CO_X$) into NiOOH nanosheets through atomic-level modification. Experimental results together with DFT calculations showed that this anionic coordination environment lowers the energy barrier for urea dehydrogenation, enabling urea to bypass the pre-formation of NiOOH and undergo a lower-energy direct oxidation process on the reconstructed Ni sites (Fig. 4a, 4b).[44] Supporting this view, Wen *et al.* constructed a Ni_2P-MoO_X heterojunction on black phosphorus nanosheets and showed that the introduction of Mo species effectively tunes the d-band center of Ni. This electronic modulation drives a shift in the UOR pathway from the conventional indirect mechanism to the kinetically more favorable direct mechanism.[56]

2.2 Product Selectivity

While the ideal product of the UOR is benign dinitrogen (N_2), the reaction in practice is often accompanied by the formation of nitrite (NO_2^-) and cyanate (NCO^-). The release of these soluble and highly toxic nitrogen-containing overoxidation products undermines the central objective of simultaneous nitrogen removal from wastewater and may lead to secondary environmental problems, including elevated aquatic toxicity and aggravated eutrophication. Tatarchuk *et al.* quantitatively analyzed the product distribution on Ni-based catalysts and showed that, under conventional alkaline electrolysis conditions, nitrite and cyanate are in fact the major products, rather than the commonly assumed dinitrogen gas. This study challenges the widespread tendency to overestimate gaseous products and highlights the need for a more rigorous re-examination of UOR product detection methods.[33] At the product level, these observations are better interpreted as competition between representative product-forming branches, as summarized in Figure 3. This scheme is based mainly on the mechanistic framework proposed by Tatarchuk et al. and is further informed by related selectivity studies on nitrite- and N_2-selective nickel-based interfaces discussed below.[5,33,57,58]

View Article Online
DOI: 10.1039/D6CC01805J

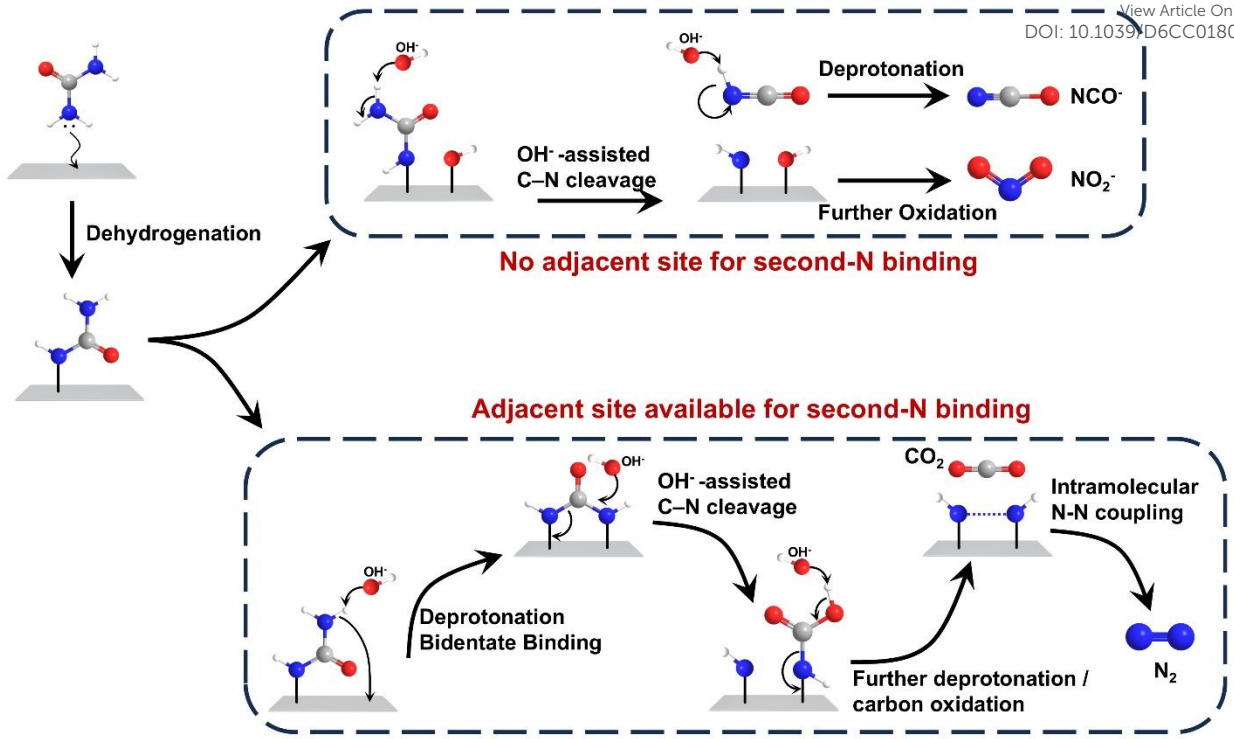

Fig. 3 Representative product-forming branches in the urea oxidation reaction at nickel-based catalytic interfaces.

To regulate product selectivity within these competing branches, researchers have explored several strategies. At their core, these approaches focus on engineering the local coordination environment and tuning the electronic structure of active sites. Such regulation alters the evolution of adsorbed urea-derived intermediates and can redirect the reaction toward surface-confined N-N coupling to form N_2, accompanied by oxidation of the carbon-containing fragment to CO2, or toward premature C-N cleavage with cyanate release and further oxidation of the remaining N-containing fragment to nitrite/nitrate. With the aim of favoring highly oxidized products and improving electron-transfer efficiency, Wang *et al.* achieved highly selective conversion of urea to nitrite by precisely tuning intermediate adsorption on Co, Ge co-doped Ni catalysts. Their results provide an important mechanistic basis for understanding directed C-N bond cleavage and pathway control in nickel-based systems (Fig. 4c-e).[57] In contrast, Shen *et al.* developed a Cu/Ni-B interface to favor N_2 formation. In this design, boron was used to construct a highly active amorphous Ni-B substrate, while Cu was introduced to moderate the excessively high density of electrophilic OH* species. The resulting interface provided enough spatial freedom for the simultaneous adsorption of two N atoms derived from a single urea molecule. This adsorption configuration promoted N-N bond coupling, while suppressing C-N bond cleavage and subsequent overoxidation, leading to an extremely high Faradaic efficiency for N_2.[58] Zhan *et al.* further designed atomically isolated asymmetric Ni-O-Ti sites on Ti foam and found that the oxophilic Ti atoms specifically anchored carbonyl oxygen species. This asymmetric configuration prevented premature cleavage of the C=N bond and instead drove the intermediates toward intramolecular N-N coupling, ultimately delivering an N_2 selectivity of 99% (Fig. 4f).[5] Guo *et al.* likewise tuned the interfacial Ni-Te bond length to 2.71 Å. The associated downward shift of the Ni d-band center promoted OH adsorption and facilitated the formation of an active Ni^{3+}-O layer, which effectively stabilized the $*H_2NCNO$ intermediate and suppressed premature C-N bond cleavage. This work further supports the view that the coordination microenvironment plays a key role in determining product selectivity, and it achieved an N_2 selectivity above 80%.[48]

2.3 The Ammonia-Intermediate and Alternative Pathways

The direct/indirect distinction mainly describes whether NiOOH is consumed and regenerated during UOR; it does not fully cover cases in which urea is first chemically dissociated or converted on spatially distinct sites. Accordingly, dual-site local mechanisms are better interpreted as alternative dissociation-oxidation pathways rather than as simple subtypes of the direct mechanism.[35] In a representative study, Geng *et al.* synthesized nickel ferrocyanide ($Ni_2Fe(CN)_6$) and, through *in situ* X-ray absorption fine structure (XAFS) spectroscopy, observed no detectable NiOOH formation during the reaction. Based on this result, they proposed a "dual-site local reaction mechanism," in which Ni sites mediate the initial chemical cleavage of urea into NH_3 intermediates, while adjacent Fe sites catalyze the subsequent electrochemical oxidation of the generated ammonia to N_2. This NH_3-intermediate pathway bypasses the energetically demanding NiOOH formation step (Fig. 5b, 5c).[35] In a related system, Cai *et al.* investigated nanoporous P-$Ni(OH)_2$ decorated with single-atom tungsten (W) and proposed a "Chemical-Electrochemical Coupled Pathway." Their results showed that the

introduction of W sites promotes the dehydrogenation of lattice hydroxyls, and the resulting active intermediates can spontaneously couple with urea molecules before undergoing electrochemical oxidation at very low overpotentials. This chemically assisted step helps alleviate the kinetic limitation imposed by the RDS in a purely electrochemical pathway.[9]

View Article Online
DOI: 10.1039/D5CC01805J

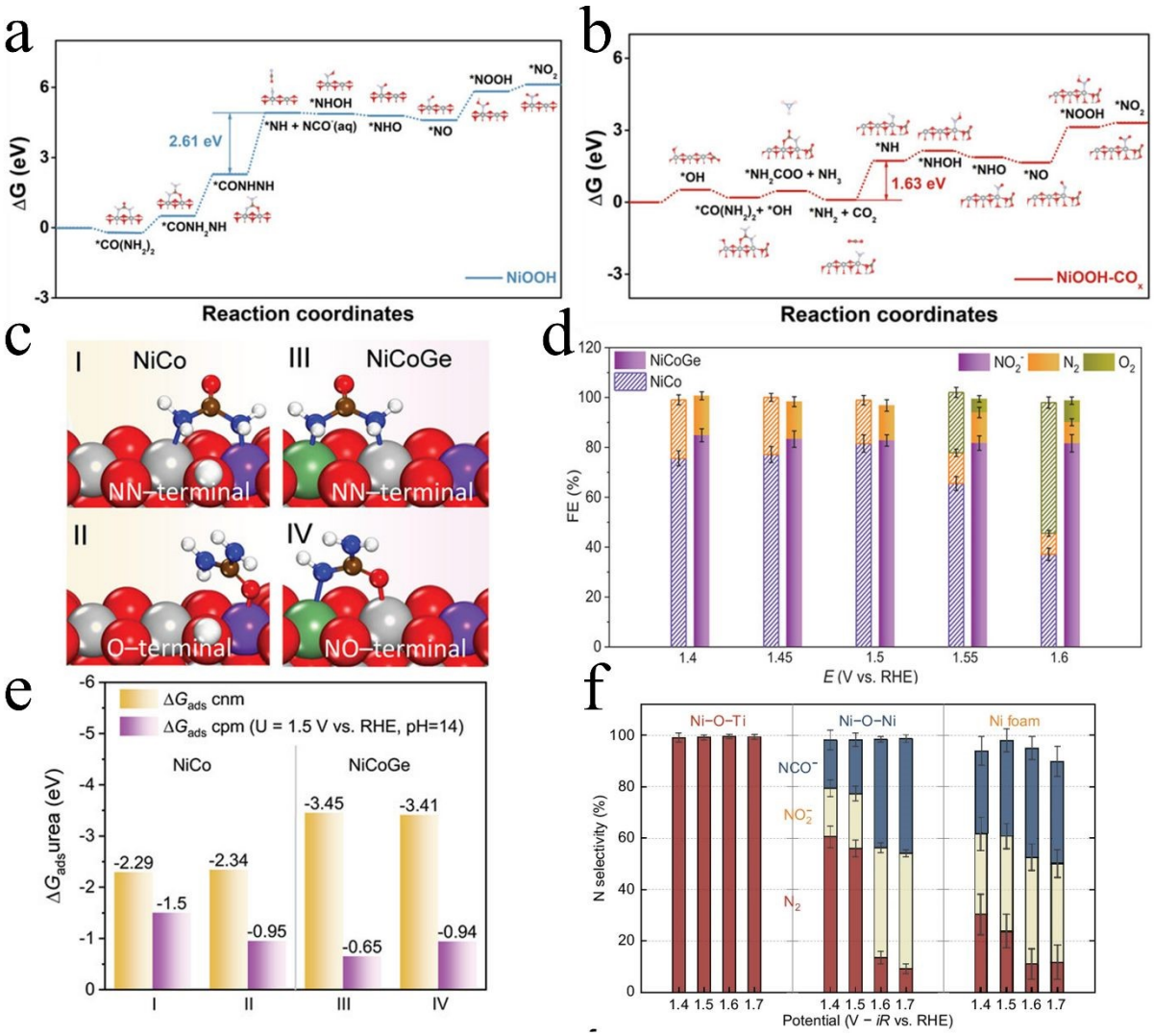

Fig. 4 The free energy diagram of the path from $CO(NH_2)_2$ to N_2O on a) NiOOH and b) NiOOH-CO_X. Reproduced from ref. 44 with permission from John Wiley and Sons, Adv. Funct. Mater., 2025, 36, e19865, copyright 2025. c) Stable structures for urea molecules adsorbed on NiCo and NiCoGe catalysts. There are two corresponding configurations for NN-terminal and O/NO-terminal adsorptions. d) Adsorption energy for urea molecule in Figure 4c is based on charge–neutral and constant potential methods (cnm and cpm). e) FEs for UOR products for NiCoGe under applied potential. Reproduced from ref. 57 with permission from John Wiley and Sons, Adv. Funct. Mater., 2023, 33, 2300687, copyright 2023. f) Selectivity of asymmetric Ni-O-Ti sites, symmetric Ni-O-Ni sites, and Ni foam as a function of applied potential; error bars represent the standard deviation from three independent samples. Reproduced from ref. 5 with permission from Springer Nature, Nat. Commun., 2024, 15, 5918, copyright 2024.

Beyond the identification of alternative pathways, the role of Fe in UOR remains under debate. In contrast to the view of Geng *et al.*, who regarded Fe as a direct active site, Zemtsova *et al.* offered a different interpretation based on systematic *in situ* characterization. They found that although incorporated Fe serves as a highly active center for the OER, its presence is unfavorable for the UOR. More specifically, Fe incorporation shifts the $Ni(OH)_2$/NiOOH redox transition to more positive potentials, while also moving the OER onset to lower potentials. As a result, parasitic OER competition becomes much more pronounced and can outcompete the UOR at high potentials. These findings suggest that Fe plays a dual role in this system: it promotes OER but hinders UOR kinetics.[59]

A separate mechanistic divergence has also been identified in studies aimed at suppressing competitive NO_X formation. Through a comparative analysis, Yang *et al.* found that conventional NiCo hydroxides tend to produce nitrite, which they attributed to the strong N-H bond activation capability of high-valence Ni^{3+}/Ni^{4+} species. By contrast, CuCo hydroxides showed much higher N_2 selectivity. *In situ* spectroscopy indicated that this behavior is

View Article Online
DOI: 10.1039/D6CC01805J

associated with the *in situ* formation of nucleophilic Cu-OO^- active sites, which promote the nucleophilic substitution of amino groups and facilitate N-N coupling (Fig. 5d).[60]

Most conventional UOR studies have focused on direct oxidation pathways in idealized alkaline electrolytes. However, practical treatment of complex waste streams, such as human urine with high chloride concentrations, poses a different challenge. Under such chlorine-rich conditions, traditional alkaline oxidation is strongly hampered by electrode and electrolyzer corrosion caused by the competing chlorine evolution reaction (ClER), especially at industrially relevant current densities. In this context, a halogen-mediated oxidation route offers a practical alternative and may help avoid NO_2^- formation in complex water matrices. To address the sluggish kinetics of conventional Cl_2-involved indirect oxidation, Wang *et al.* demonstrated a kinetically favorable "Cl-Mediated Mechanism" on Pt catalysts in acidic urine systems. In this pathway, adsorbed chlorine (Cl*) directly couples with urea to form N-chlorourea intermediates. This fast mediated oxidation route turns chloride from a source of corrosion into a reactive participant, enabling efficient dinitrogen (N_2) production through intermolecular N-N coupling (Fig. 5e).[4]

These results, however, should be distinguished from the broader matrix tolerance required for NiOOH-based UOR in practical effluents. In alkaline NiOOH systems, organic constituents and competing ions may perturb the formation–consumption balance of reconstructed NiOOH by site blocking, complexation, precipitation, or side redox reactions. Recent studies using real urine or urine-relevant matrices indicate that creatinine, histidine, and creatine can compete with urea adsorption on Ni(III) sites, whereas Mg^{2+}/Ca^{2+} and Cl^- can introduce precipitation, poisoning, or corrosion issues under alkaline operation.[4,61] Heavy-metal ions in industrial or mixed effluents represent an additional, less systematically examined factor; at polarized interfaces, they may undergo electroadsorption, redox conversion, or precipitation, which could alter the local NiOOH microenvironment.[62] Such matrix effects may change the lifetime and coverage of NiOOH-derived sites and thereby shift the balance among urea activation, OER/Cl chemistry, and overoxidation pathways toward NO_2^- and NCO^-.[5,33] Consequently, long-term selectivity should be assessed by coupling operando tracking of NiOOH reconstruction with matrix-matched product analysis (e.g., IC, GC, DEMS, and NMR) rather than by activity retention alone.

2.4 Evolution of Key Intermediates and the Rate-Determining Step (RDS)

The sluggish kinetics of the UOR arise from the complex evolution of reaction intermediates, including species such as *CO, *COO, and *NCO, as well as from unfavorable scaling relations that are difficult to overcome. A clear identification of intermediate configurations and the rate-determining step (RDS) is therefore essential for understanding and controlling product selectivity. In this context, capturing key adsorbed intermediates and clarifying the associated RDS are central to the rational design of advanced catalytic materials. By tuning the electronic structure and local coordination environment of active sites to optimize the binding energies of these intermediates, it becomes possible to alleviate thermodynamic scaling constraints, accelerate the intrinsic reaction kinetics, and steer the overall reaction pathway.

For the analysis of adsorption configurations, An *et al.* used *in situ* attenuated total reflection surface-enhanced infrared absorption spectroscopy (ATR-SEIRAS) to directly monitor the dynamic configurational evolution of urea on Ni film electrodes. They showed that urea initially adopts an O-terminal adsorption mode at open-circuit potential, and then rotates at higher potentials to form an N-terminal active configuration. By capturing key species such as *NCO (Fig. 5a), they proposed that the complete oxidation pathway follows the sequence *$OC(NH_2)_2$ *NH_2CONH_2 *NCO\N_2, thereby clarifying the importance of adsorption-configuration evolution in the UOR process.[41] To further optimize this adsorption behavior, Yin *et al.* constructed a NiTe/Mo_6Te_8 heterojunction with spontaneous electronic rearrangement. They found that a polarized interfacial microenvironment was formed, in which nucleophilic sites preferentially adsorb the N-terminus and electrophilic sites preferentially adsorb the O-terminus. The synergistic action of these distinct sites markedly lowers the energy barrier for dual-terminal adsorption.[63]

At the level of intermediate evolution, the energy barrier of the RDS largely determines the overall UOR kinetics. To address the sluggish *CO-N*CO·OH step commonly encountered in conventional pathways, Feng *et al.* developed a WN/Ni_3C composite coating. Their experimental and theoretical results indicated that strong interfacial electron transfer from WN to Ni_3C enhances electron injection from the catalytic sites into adsorbed urea intermediates. This electronic regulation improves the adsorption energetics of *CO-N_2 species, lowers the activation barrier of the RDS, and accelerates the overall electro-oxidation process.[64]

The identification and regulation of the RDS have also been examined from the perspective of intermediate binding strength. Chen *et al.* synthesized P- and W-co-doped carbon-encapsulated NiCo composites and combined experimental observations with theoretical calculations to analyze the binding energies of key intermediates. They found that the overly strong interaction between high-valence Ni^{3+} and *COO impedes *COO desorption, which they identified as the genuine RDS governing the performance of most nickel-based catalysts. Heteroatom incorporation effectively weakens this poisoning effect.[65] In a different strategy, Chen *et al.* reported an "adaptive active site turning" mechanism in the Ir-Ni_3N system. Rather than operating through a static active center, the Ir and Ni dual sites dynamically switch and cooperate under the specific UOR environment. This adaptive electronic response tunes the binding strength of key nitrogen-containing intermediates, avoiding both excessive binding that causes poisoning and overly weak binding that limits activation. As a result, the activation barrier of the RDS is reduced and the electro-oxidation cycle proceeds more efficiently.[66] Wu *et al.* further showed that strengthening targeted adsorption while simultaneously providing an oxygen source is an effective way to construct a highly active UOR interface. Using MoO_4^{2-}-doped NiCo layered double hydroxides (LDHs), they proposed a "self-adaptive adsorption" mechanism in which the catalyst dynamically adjusts the adsorption behavior of hydroxyl (OH^-) intermediates depending on whether urea is present. This endows the bifunctional catalyst with the ability to switch active sites in response to the reaction environment. During the UOR, this dynamic

site regulation preferentially strengthens OH^- adsorption on Co sites. The resulting local enrichment not only lowers the kinetic barrier, but also supplies a direct oxygen source for the deep oxidation of urea, thereby improving the intrinsic catalytic turnover.

View Article Online
DOI: 10.1039/D6CC01805J

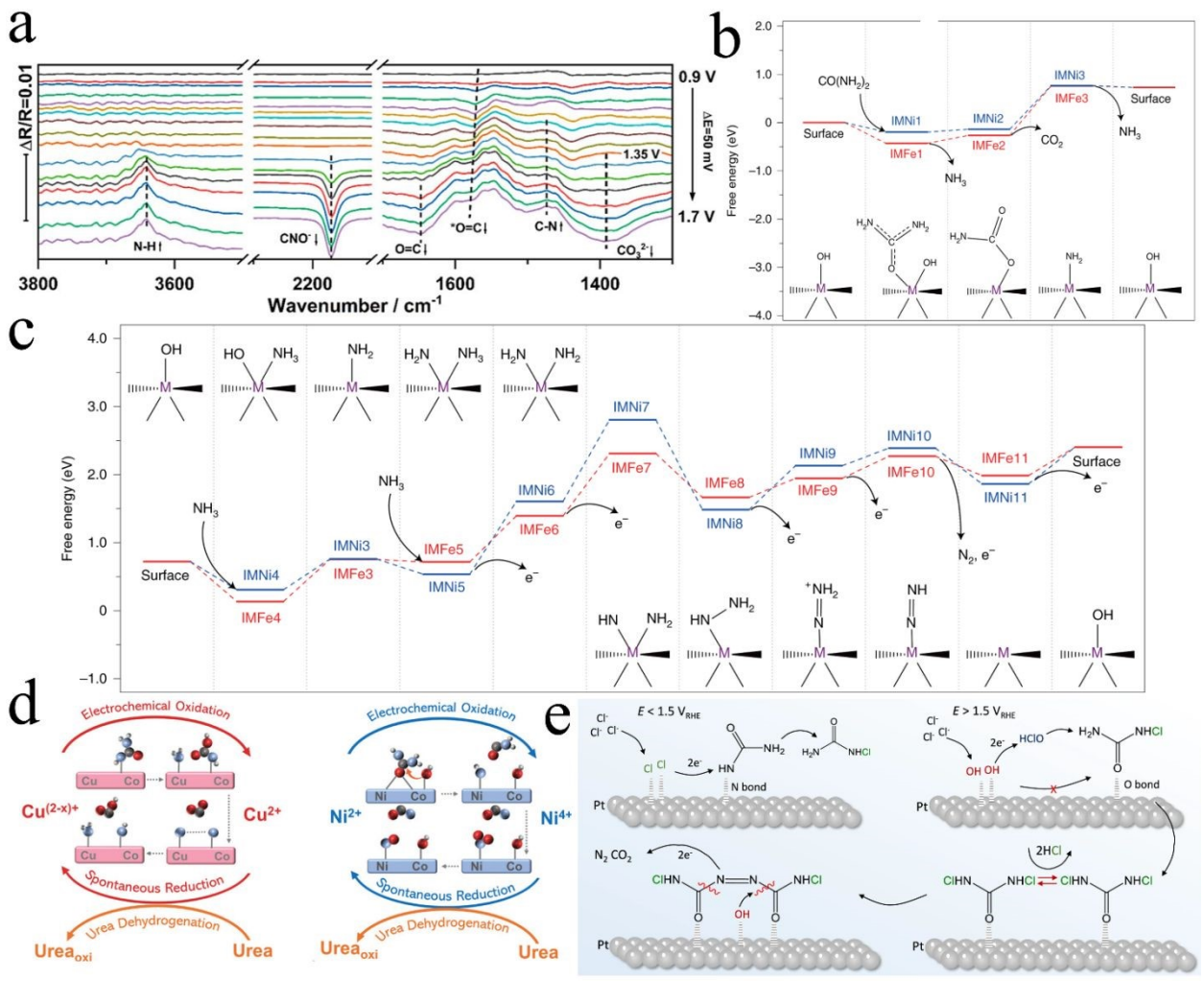

Fig. 5 a) *In situ* ATR-SEIRAS spectra on a Ni film electrode recorded from 0.9 V to 1.7 V (vs. RHE) in 1 M KOH + 0.33 M urea; the reference potential is set at 0.9 V, and arrows indicate the direction of infrared peak intensity changes. Reproduced from ref. 41 with permission from American Chemical Society, J. Phys. Chem. C, 2023, 128, 77-84, copyright 2023. (b,c) The Gibbs free energy diagrams of a two-stage UOR (that is, the reaction from urea to NH_3 (b) and the reaction from NH_3 to N_2 (c)) on both the Fe and Ni sites of the $Ni_2Fe(CN)_6$ catalyst. Arrows in the reaction channels indicate the reactants or products involved (H_2O and OH^- are omitted), and e^- represents an electrochemical step. The initial structures of the active sites, that is, Fe or Ni on the $Ni_2Fe(CN)_6$ surface, are hydroxylated (M·OH) because hydroxylation is a spontaneous reaction at a 1.35 V working potential, that is, $\Delta rG^\circ_m = -0.93$ eV (0.42 eV − e × U). The adsorption of OH^- facilitates the binding of the reactants with the catalyst because the atomic charge of the active sites increases. Reproduced from ref. 35 with permission from Springer Nature, Nat. Energy, 2021, 6, 904-912, copyright 2021. d) A schematic illustration of urea oxidation pathway and structural transformation on CuCo(left) and NiCO(right),respectively. Reproduced from ref. 60 with permission from John Wiley and Sons, Adv. Mater., 2024, 36, 2403187, copyright 2024. e) Schematic illustration of the whole reaction mechanism for Cl-UOR on Pt for conversion of urea to N_2. Reproduced from ref. 4 with permission from Springer Nature, Nat. Commun., 2025, 16, 2424, copyright 2025.

3. Dynamic Reconstruction and Active Sites

Although nickel-based materials are extensively utilized in the UOR, the genuine catalytic active phase under operating conditions often diverges significantly from the initial synthesized state (pre-catalyst). Recent studies emphasize that comprehending the dynamic surface reconstruction of the catalyst, capturing high-activity metastable species, and elucidating the role of lattice oxygen participation are pivotal to unveiling the underlying structure-activity relationships in UOR. Furthermore, this dynamic surface reconstruction is not only

View Article Online
DOI: 10.1039/D6CC01895J

the origin of catalytic activity but also crucial for long-term UOR stability, as an appropriate reconstructed layer protects against active species leaching. Conversely, excessive structural transformation leads to mechanical degradation and rapid performance decay.

3.1 Surface Reconstruction from Precatalysts to Active Phases

The vast majority of nickel-based compounds, including sulfides, phosphides, MOFs, and oxides, undergo irreversible surface reconstruction under alkaline UOR potentials and are transformed *in situ* into highly active metal (oxy)hydroxide layers. This process is commonly accompanied by lattice collapse, sacrificial anion dissolution, and the formation of an amorphous active shell.

Using the classic $NiMoO_4$ system as a model, Zhu *et al.* combined cryogenic transmission electron microscopy (Cryo-TEM) with *in situ* Raman spectroscopy to follow the multistep dissolution and reconstruction of layered $NiMoO_4$ crystals. Their results showed that the dissolution of Mo species and crystalline water drives the collapse of the original crystal framework and its *in situ* conversion into superthin amorphous $Ni(OH)_2$ floccules (Fig. 6a-c). Notably, this reconstructed amorphous phase exhibits a lower oxidation potential than directly synthesized crystalline counterparts, indicating the higher activity of the reconstructed phase. Although amorphous structures are often considered unfavorable for bulk charge transport, electrochemical measurements showed that this amorphous catalyst in fact displays much faster charge-transfer kinetics than its well-crystallized counterpart. Zhu *et al.* attributed this behavior to the combined effect of structural disorder and ultralow thickness. Rather than hindering electron transport, the superthin flocculent architecture exposes abundant active sites and facilitates the real-time generation of high-valent Ni species, thereby improving interfacial charge transfer and accelerating UOR kinetics.[68] To capture this phase transition in real time, Dürr *et al.* developed a time-resolved *in situ* Raman platform to monitor the electrochemical activation of the $NiMoO_4$ precatalyst. They observed that, once anodic bias was applied, the Mo-O vibration peaks in the low-frequency region gradually weakened, whereas the characteristic γ-NiOOH peaks in the high-frequency region quickly appeared (Fig. 6d, 6e). This spectral evolution confirms that the bimetallic precursor undergoes electrochemically driven leaching of the soluble Mo component, followed by an irreversible *in situ* transformation into the genuine catalytically active phase.[53]

The role of anions in reconstruction kinetics has also attracted considerable attention. Bao *et al.* studied Mo-Ni_3S_2 nanowire arrays and found that lattice S and Mo are first oxidized and leached into the electrolyte as sulfite and molybdate. Importantly, these anions do not simply act as sacrificial species. Instead, they can re-adsorb onto the newly formed NiOOH shell. This dynamic "leaching-and-readsorption" process gives rise to a highly active phase, in which surface co-adsorption tunes the d-band center of Ni sites and thereby optimizes the adsorption energetics of key UOR intermediates, such as $*CON_2$.[69] In a similar vein, Chen *et al.* observed pronounced boron leaching in Ni_2B nanoflakes during the transition from precatalyst to active phase. Their results showed that electrochemical boron dissolution is a key driving force for surface reconstruction. Rather than generating a conventional bulk phase, this dynamic process converts the precursor into a highly porous, vacancy-rich NiOOH active phase with abundant exposed active sites and improved adsorption kinetics for reactive species.[70] Bai *et al.* further examined the surface reconstruction of $NiMoO_4$ nanowires and used fluorine (F) anion doping to regulate the phase transition. They found that surface-localized F dopants dynamically mediate the balance between NiOOH generation and depletion. This regulation suppresses excessive accumulation of the NiOOH active phase, thereby inhibiting competing OER while maintaining efficient interfacial UOR kinetics.[71]

In addition to anions, cation doping can also markedly accelerate surface reconstruction. Wang *et al.* showed that Ce doping in Ni_5P_4 induces electron transfer from P and Ni to Ce. This electronic modulation not only increases the valence state of Ni, but also promotes the reconstruction of the Ni_5P_4 surface into highly active NiOOH species, thereby strengthening intermediate adsorption on the (210) crystal plane.[72] Such phosphide-based examples are consistent with recent analyses of nickel phosphide precatalysts, which suggest that precursor chemistry and surface evolution should be considered together when rationalizing their high UOR activity.[73] For more complex metal-organic framework (MOF) precatalysts, Ge *et al.* proposed an "environmental reconstruction" strategy to overcome the limitations of conventional activation. They showed that undercoordinated 2D CoNi-MOFs reconstruct in the electrolyte into a CoNi-MOF@$CoNi(OH)_2$ architecture. This reconstruction introduces abundant oxygen defects, which improve urea adsorption and allow the UOR to be initiated before the kinetically sluggish Ni self-oxidation reaction (NSOR) occurs. In this way, the conventional evolutionary pathway from precatalyst to active phase is substantially altered.[24] In heterojunction systems, Wang *et al.* designed a Ni/MnO heterojunction catalyst and observed an unusual phenomenon of "two successive surface reconstructions". Their results showed that the incorporation of heterocomponents such as Mn can significantly reshape the thermodynamic landscape of Ni reconstruction, driving a cascade of surface phase transitions from $Ni(OH)_2$/MnOOH to NiOOH/MnOOH and ultimately leading to stepwise enhancement of catalytic activity.[74]

Taken together, these diverse reconstruction behaviors point to a common conclusion: for deeply reconstructed interfaces, the initial electrochemical activation stage is far more than a routine pretreatment. It is a key evolutionary step that strongly affects both the final catalytic activity and the long-term stability. A well-controlled activation process determines the depth, pathway, and kinetics of sacrificial leaching and phase transformation, and thereby governs the conversion of precursors into optimal high-valent active species with suitable vacancies and porosity. Careful regulation of this early-stage reconstruction can also reduce the risk of severe volume expansion, active-layer shedding, and excessive mechanical pulverization. Importantly, the stability penalty associated with reconstruction should not be viewed as an inevitable consequence of reconstruction itself. A thin and electronically connected NiOOH-derived shell may support sustained UOR, whereas excessively deep or poorly confined reconstruction can generate a mechanically fragile active-layer. Continuous sacrificial-anion leaching, repeated $Ni^{2+}/Ni^{3+}/Ni^{4+}$ cycling, partial dissolution of doped metals, and local stress associated with lattice collapse may progressively weaken the

View Article Online
DOI: 10.1039/D6CC01805J

contact between the active shell and the conductive scaffold. At ampere-level current densities, the higher anodic potentials required to sustain rapid urea conversion can further intensify OER competition and may promote over-oxidation or passivation of NiOOH-derived phases; rapid gas evolution and steep local concentration gradients may also amplify interfacial stress and accelerate active-layer shedding. Thus, unsatisfactory UOR durability is better interpreted as a coupled consequence of active-phase evolution, component leaching, competing side reactions, and current-induced interfacial stress, rather than as a single deactivation pathway.[32,43,46,54,59,70-72]

3.2 High-Valent Ni Species

Regarding the active sites for the UOR, a long-standing debate has centered on the respective roles of Ni^{3+} species, typically represented by γ-NiOOH, and higher-valence Ni^{4+} species. In most Ni-based systems, NiOOH is generally regarded as the principal active phase, and its catalytic function is closely associated with the strong ability of high-valence Ni centers to activate urea molecules. Using amorphous NiNb nanoglass as a precursor, Sohel *et al.* identified the stable γ-NiOOH phase by *in situ* Raman spectroscopy. Their results showed that, compared with the conventional β-NiOOH phase, γ-NiOOH, with its larger interlayer spacing and higher oxidation state, is more closely associated with efficient direct urea oxidation.[26] To further track the evolution of high-valence Ni species, Ge *et al*. combined *in situ* Raman spectroscopy with synchrotron X-ray absorption spectroscopy (XAS). In pure alkaline electrolyte, the Ni K-edge shifted markedly toward higher energy, indicating oxidation to an average valence state above +3. Under actual UOR conditions, however, this high-valence spectral feature disappeared completely. This spectral change suggests that the high-valence Ni species generated during polarization are rapidly consumed during urea oxidation, supporting the view that Ni^{3+}-related centers are directly involved in the catalytic process (Fig. 7a, 7b).[75]

High-valence Ni sites, however, are often vulnerable to over-oxidation and dissolution during electrocatalysis. To address this issue, Zhang *et al.* proposed a "dynamic regeneration" strategy based on V-modified NiCo oxides. In this system, stable high-valence V^{5+} species do not function as sacrificial components, but instead serve as co-catalytic sites that preferentially adsorb *OH. This, in turn, assists adjacent high-valence Ni^{3+} centers in promoting C-N bond cleavage and accelerates the urea dehydrogenation step. As a result, Ni^{3+} can be rapidly reduced back to Ni^{2+}, which helps suppress excessive oxidation of NiOOH and sustain the continuous generation of catalytically active high-valence Ni species (Fig. 7c).[54] Along similar lines, Kovilakath *et al.* compared the UOR behavior of conventional $Ni(OH)_2$ and $Ni_3O_2(OH)_4$, and found that highly crystalline (oxy)hydroxides could maintain stable Raman signals associated with high-valence species throughout the reaction. This result indicates that catalyst durability depends not only on resistance to poisoning, but also on the dynamic replenishment rate of the NiOOH regenerative active species consumed at the surface during operation.[21] Li *et al.* further showed, using plasma immersion ion implantation, that suppressing deep deprotonation of the $Ni(OH)_x$ surface can prevent conversion of the active γ-NiOOH phase into the UOR-passivated NiOO phase. This finding highlights that inhibiting over-oxidation of the surface active phase is critical for maintaining sustained UOR activity.[32]

3.3 Dynamic Activation of the Lattice Oxygen Mechanism (LOM)

Traditional adsorbate evolution mechanisms (AEM) generally assume that catalytic reactions occur exclusively at metallic sites on the catalyst surface.[76] Relative to the direct/indirect framework discussed above, LOM can be considered a direct surface-oxidation route in a broad sense because the oxidation of urea-derived intermediates proceeds at high-valent metal–oxygen units without a stoichiometric NiOOH-to-$Ni(OH)_2$ regeneration step. However, it should be distinguished from the conventional direct adsorbate-evolution pathway, because lattice oxygen participates as an oxygen source and the generated oxygen vacancies must be replenished by electrolyte OH^-.[36] Within this classical framework, the UOR proceeds through a series of elementary steps, including urea adsorption, N-H dehydrogenation, and C-N bond cleavage.[30] Among them, CO_2 desorption is commonly considered the rate-determining step because of its high energy barrier. As a result, although AEM offers a relatively well-defined catalytic cycle, the overall reaction kinetics remain sluggish, and the catalyst is prone to deactivation or poisoning by strongly adsorbed CO_2 species. By contrast, in nickel-based systems with strong metal-oxygen covalency and high-valence active sites, such as Ni^{4+}, lattice oxygen can be activated and directly participate in the oxidative bond-cleavage process of urea. In this lattice oxygen mechanism (LOM), surface lattice oxygen reacts with intermediates to generate oxygen vacancies, which are then replenished by hydroxyl ions from the electrolyte. A key advantage of this pathway is that it can bypass the severe CO_2 desorption limitation associated with AEM, thereby accelerating the overall reaction kinetics. This kinetic benefit, however, may also raise durability concerns if lattice oxygen participation is not sufficiently reversible or structurally buffered. Continuous participation, consumption, and replenishment of lattice oxygen may gradually perturb the nanocatalyst framework and compromise long-term electrochemical stability.

View Article Online
DOI: 10.1039/D6CC01805J

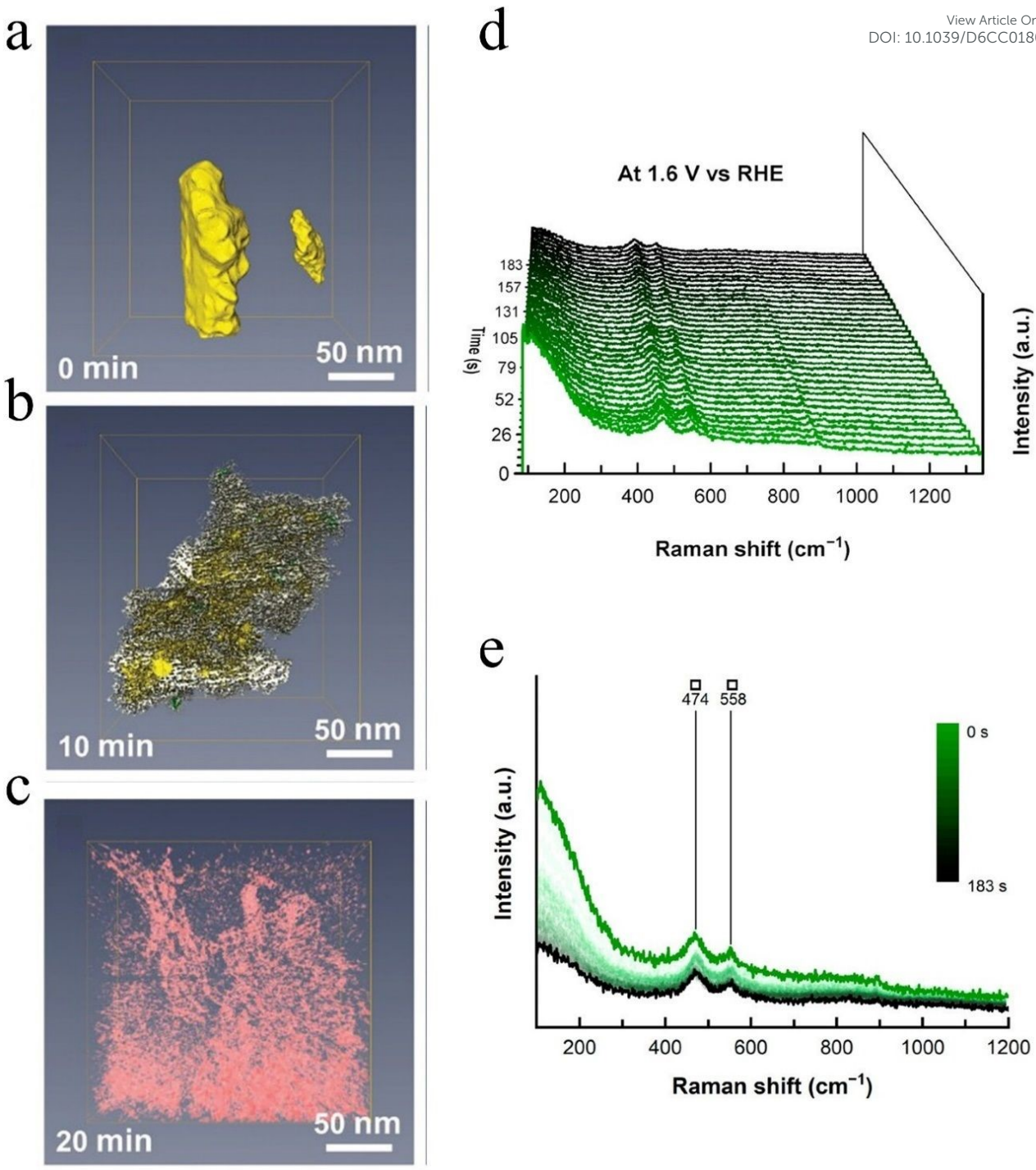

Fig. 6 CryoET reconstructed 3D models of $NiMoO_4 \cdot H_2O$ dissolved in alkaline solution for a) 0 min, b) 10 min and c) 20 min, respectively.Bulk $NiMoO_4 \cdot H_2O$ crystals are in yellow, exfoliated $NiMoO_4 \cdot xH_2O$ nanosheets are in white and green, and ANH flocculus are in red. Reproduced from ref. 68 with permission from John Wiley and Sons, Adv. Mater., 2023, 35, 2301549, copyright 2023. Time resolved *in situ* Raman spectroscopy at 1.6 V vs RHE of $NiMoO_4$@Nif-2, d) 3D plot of the single spectra with the first acquisition at the very front and the last acquisition after 183 s at the very back. e) The same data illustrated in a 2D plot, displaying the presence of majorly γ-NiOOH vibrations (□),The small signal at 896 cm^{-1} is from a monomolybdate in solution. Reproduced from ref. 53 with permission from American Chemical Society, ACS Nano, 2021, 15, 13504-13515, copyright 2021.

To verify the mechanistic advantages of LOM and to make use of this pathway in catalyst design, considerable effort has been devoted to capturing direct evidence for lattice oxygen participation and to engineering catalyst structures that favor this highly efficient route. In 2019, Zhang *et al.* reported a lattice-oxygen-involved reaction pathway, here referred to as the lattice oxygen mechanism (LOM), in which Ni^{4+}-rich species formed under strong anodic polarization dynamically activate lattice oxygen. By combining ^{18}O

View Article Online
DOI: 10.1039/D6CC01805J

isotope-labeling secondary-ion mass spectrometry (SIMS) with *in situ* FTIR spectroscopy, they directly observed oxygen exchange between the catalyst lattice and the electrolyte, together with the facile generation of CO_2 products (Fig. 7d, 7e). These results provide direct experimental support for the participation of activated lattice oxygen in the oxidation of C=O-related intermediates to CO_2. Because this pathway avoids the kinetic constraint associated with CO_2 desorption in conventional Ni^{3+}-mediated routes, it markedly accelerates UOR kinetics and leads to an approximately fivefold increase in the turnover frequency (TOF) of Ni active sites.[36] To deliberately induce and further enhance this efficient LOM pathway, Han *et al.* developed a chemical delithiation strategy to introduce controllable cation vacancies into layered $LiNiO_2$ oxides. Synchrotron-based spectroscopies combined with *in situ* FTIR analyses showed that a moderate concentration of cation vacancies triggers charge disproportionation at Ni sites, generating more Ni^{4+} species and strengthening Ni-O covalency (Fig. 7f). This electronic regulation activates lattice oxygen and facilitates the electrochemical deprotonation steps of the UOR, thereby lowering both the reaction barrier and the overpotential. These results further identify defect engineering as an effective atomic-scale strategy for activating the lattice oxygen mechanism.[77] These observations are also consistent with the review by Zhang *et al.*, which concluded that rational regulation of metal-oxygen covalency to trigger the LOM is a key direction for overcoming the catalytic efficiency limitations of the UOR.[76]

Taken together, the desirable regime is not unrestricted lattice-oxygen turnover, but a controlled LOM contribution that remains compatible with framework integrity. While lattice-oxygen participation can accelerate UOR by bypassing the sluggish CO_2 desorption step, excessive oxygen-vacancy generation and refilling may progressively amplify local bond reorganization, lattice disorder, and interfacial stress, thereby destabilizing the reconstructed Ni-O framework under sustained anodic operation. Conversely, overly suppressing lattice reactivity may preserve structural integrity at the expense of turnover efficiency. The practical design target is therefore better interpreted as a dynamically replenishable metal-oxygen network that can sustain partial lattice-oxygen participation without triggering deep structural collapse. This consideration also helps rationalize the regulation strategies discussed below.In this sense, a sustainable LOM regime is better interpreted as controlled lattice-oxygen participation sustained by sufficiently robust metal-oxygen networks.

4. Interface Regulation Strategies

To overcome the intrinsic bottlenecks of sluggish kinetics involving six-electron transfer and the masking of active sites by gaseous products in the nickel-based urea oxidation reaction (UOR), researchers have developed hierarchical interface engineering strategies spanning from the atomic to the macroscopic scale. These strategies aim to establish profound structure-activity relationships by optimizing the intrinsic electronic structure to modulate adsorption energies, leveraging interfacial electric fields at heterojunctions to accelerate charge transfer, and reshaping the electrode microenvironment to enhance mass transport. These levels of regulation should be viewed as interrelated rather than mutually exclusive, because structural motifs, electronic states, and local reaction environments often influence each other during UOR operation.[43,78-80]

4.1 Electronic Structures: From d-Band to Spin States

Beyond lattice oxygen activation, heteroatom doping has emerged as an effective strategy for regulating the electronic structure of Ni-based UOR catalysts. Jin *et al.* used DFT calculations to compare Mn, Fe, Co, and Cu dopants in the β-$Ni(OH)_2$/β-NiOOH couple, and found that Mn and Fe are particularly effective in lowering the dehydrogenation free energy required for the formation of active β-NiOOH, while also strengthening urea adsorption on defective β-NiOOH surfaces. This improvement cannot be simply attributed to an upward shift of the Ni d-band center. Instead, it is more reasonably understood in terms of dopant-induced redistribution of Ni d states and the resulting optimization

View Article Online
DOI: 10.1039/D6CC01805J

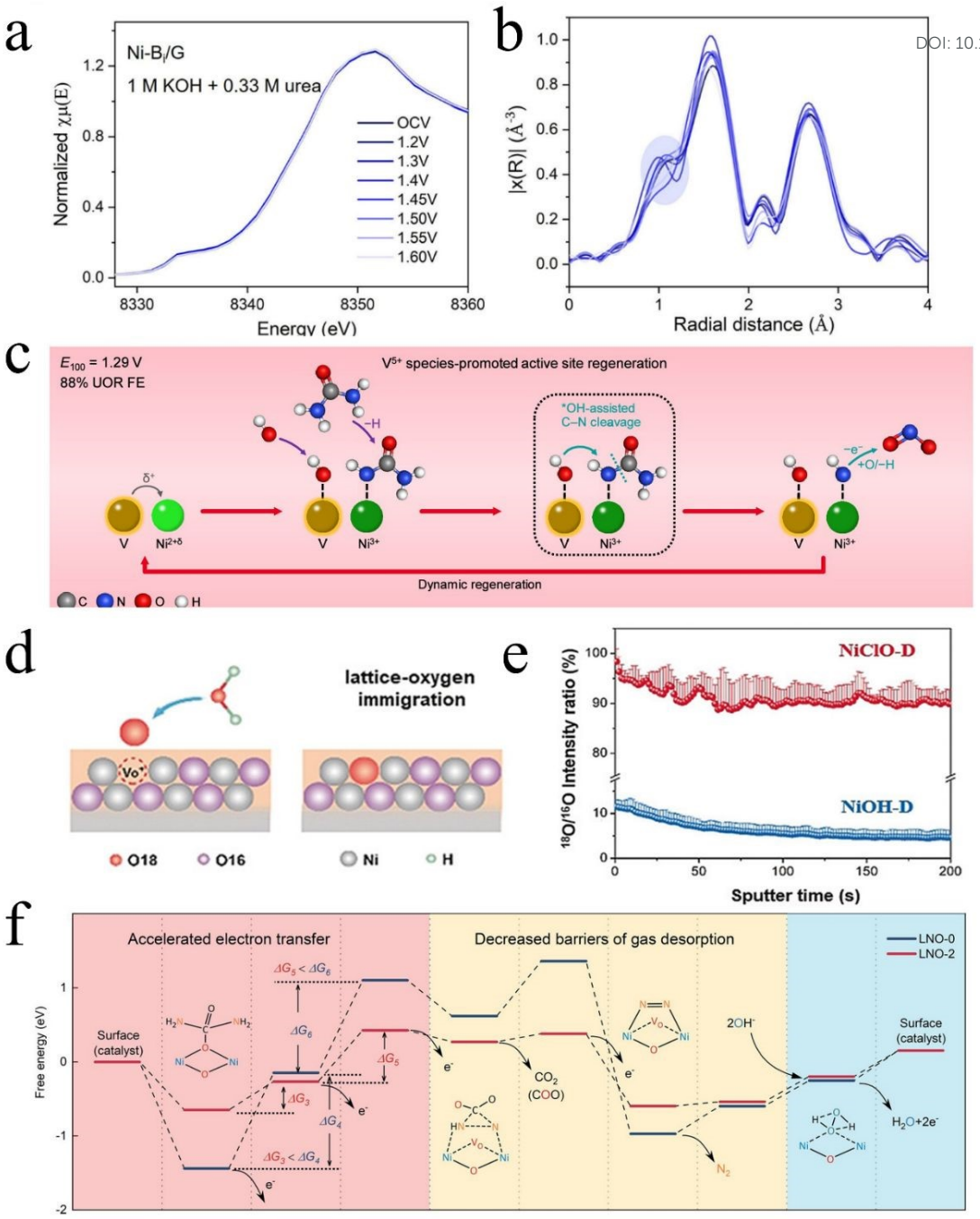

Fig. 7 a) Ni K-edge *In situ* XANES spectra of Ni-Bi/G at various potentials in 1 M KOH and 0.33 M urea and b) the corresponding Ni K-edge in R-space. Reproduced from ref. 75 with permission from Elsevier, Surf. Interfaces, 2025, 76, 107984, copyright 2025. c) Schematic illustration of high-valence vanadium species-promoted active site regeneration in the UOR, where pentavalent vanadium in $NiCoVO_x$ modulates the Ni electronic structure to facilitate active NiOOH formation and serves as an OH adsorption site to promote C–N bond cleavage and spontaneous Ni^{3+} dehydrogenation, thereby regenerating Ni^{2+} catalytic sites. Reproduced from ref. 54 with permission from American Chemical Society, ACS Catal., 2025, 15, 3143-3152, copyright 2025. d) Illustration of lattice-oxygen involvement during UOR. e) Secondary-ion mass spectrometry of the NiClO-D and NiOH-D catalysts after reaction in $H_2{}^{18}O$ aqueous electrolyte. Reproduced from ref. 36 with permission from John Wiley and Sons, Angew. Chem. Int. Ed., 2019, 58, 16820-16825. copyright 2019. f) Free energy profiles of the LOM mechanism pathway on the (003) plane for LNO-0 and LNO-2. Reproduced from ref. 77 with permission from John Wiley and Sons, Angew. Chem. Int. Ed., 2022, 61, e202206050, copyright 2022.

of the relative energetics of the UOR and OER, which together enable urea oxidation at lower overpotentials (Fig. 8a, 8b).[78] From a theoretical perspective, C_2N-supported Ni-based dual-metal-atom models further suggest that pairing Ni with a second transition-metal atom can optimize the adsorption energetics of urea-derived

View Article Online
DOI: 10.1039/D6CC01805J

intermediates and reduce the limiting potential for urea electrooxidation.[81] Going beyond conventional transition-metal regulation of Ni electronic states, Qiang *et al.* introduced a La_2O_3 interface into three-dimensionally ordered macroporous (3DOM) NiO and constructed a distinctive La-O-Ni electron bridge. Combined *in situ* spectroscopies and DFT calculations showed that this interfacial bridge redistributes local electron density and promotes the generation of high-valence $Ni^{\delta+}$ ($\delta > 3$) species at lower potentials, thereby activating the high valence nickel mechanism (HNM). More importantly, the La-O-Ni structure strengthens C=O adsorption and lowers the barrier for the potential-determining N-H bond-cleavage step, leading to faster UOR kinetics.[47]

To couple electronic-structure optimization with catalyst durability, Chen *et al.* developed a P/W co-doping strategy combined with carbon encapsulation to construct P-W-NiCo@C. Compared with the mono-doped counterparts, the synergistic incorporation of P and W modulates the local electronic structure of Ni/Co sites, shifts the d-band center upward, and promotes charge transfer as well as urea adsorption. At the same time, the outer carbon shell protects the alloy core from electrolyte corrosion and improves structural stability under UOR conditions.[65] In recent years, regulation of electronic structure has further extended from conventional d-band engineering to spin-state control. Wang *et al.* showed that photoexcitation in a Mo-doped Ni_3S_2 system induces a light-triggered transition of Ni(III) species from a low-spin to a high-spin state. ESR, *in situ* FTIR, and DFT analyses indicated that the resulting high-spin configuration strengthens the hybridization between Ni 3d and N 2p orbitals and enhances urea adsorption on the reconstructed Mo-NiOOH active phase (Fig. 8c). This spin-state modulation does not primarily facilitate C-N bond cleavage. Instead, it suppresses the thermodynamically unfavorable NO_2^-/CNO^- pathway and directs the UOR toward the more favorable N_2/CO_2 route, thereby accelerating the overall reaction kinetics.[10]

4.2 Coordination Asymmetry and Defect Engineering

Within this interrelated framework, the catalytic roles of coordination asymmetry and defect engineering are better rationalized by the anisotropic coordination motifs, vacancy-defined sites, and cooperative adsorption environments that they create, together with the accompanying local electronic redistribution. In this context, breaking local coordination symmetry has become an important strategy for constructing highly active anisotropic sites.[43,82] Li *et al.* developed a monolayer asymmetrically coordinated NiCoMn heterotrimetallic atom-site catalyst (A-NiCoMn-TAC/LDH). XAFS analysis showed that oxygen vacancies, metal vacancies, and lattice distortion jointly generate asymmetric Ni–Co–Mn coordination motifs (Fig. 8d, 8e). This distinctive local structure strengthens polymetallic synergy and, together with dynamic structural adaptation under electrochemical conditions, gives the catalyst remarkable durability, allowing stable operation for 600 h at 500 mA cm^{-2} in half-cell tests and 1500 h at 1000 mA cm^{-2} in an AEM electrolyzer.[43] A similar strategy was reported by Liu *et al.*, who engineered asymmetric Ce–O–Ni sites in a self-supported Ce-doped Ni-BDC MOF grown on nickel foam. *In situ* spectroscopy and DFT calculations showed that, after reconstruction into Ce-γ-NiOOH, Ce_{3d}-O-Ni_{2p} orbital hybridization shifts the d-band center to −1.359 eV and stabilizes the *CO intermediate. This favors the formation of COOH and lowers the barrier for the subsequent oxidation steps, thereby accelerating the overall UOR kinetics.[82]

Another effective design concept is to assign different functional roles to distinct sites within a single catalyst, so that reactant adsorption and subsequent oxidation no longer compete on one center. Following this idea, Zhou *et al.* introduced low-valence Mo^{4+} into the NiS lattice to construct Mo–Ni dual active centers. Combined *in situ* characterizations and theoretical calculations revealed a reactant-mediation mechanism, in which the Mo^{4+} sites, characterized by empty d-orbitals, preferentially adsorb urea, while adjacent Ni sites mediate the subsequent dissociation, intermediate evolution, and product desorption steps. In this way, Mo incorporation overcomes the intrinsically weak urea affinity of pristine NiS and accelerates the overall UOR kinetics.[83]

Structural-disorder engineering provides another route for regulating the local coordination environment and intrinsic catalytic properties. Zhang *et al.* synthesized amorphous nickel–iron hydrogen phosphites with tunable Fe contents. The amorphous framework provides abundant unsaturated coordination sites and low-coordination defect sites, while Fe incorporation reconstructs the local coordination environment and electronic structure. XAS and DFT analyses further showed that Fe induces an upward shift of the Ni d-band center, indicating that amorphization combined with compositional tuning can effectively regulate the intrinsic catalytic properties of nickel phosphites in urea-assisted electrolysis.[84]

Lattice-defect engineering remains a classical and versatile strategy for creating undercoordinated local motifs and increasing active-site density, often with accompanying redistribution of the local electronic structure. Mannu *et al.* showed that Mo doping can markedly promote the formation of abundant oxygen vacancies in Co_3O_4. These defect sites regulate the valence state and local electronic structure of Co, while also facilitating the adsorption of electrolyte-derived oxygen species, the pre-oxidation of low-valence Co, surface reconstruction, and the subsequent deprotonation of CoOOH-related species.. As a result, the required anodic potential is lowered and urea electrolysis performance is improved.[85] Chen *et al.* further reported an amorphous SeO_X-covered $Ni(OH)_2$ catalyst enriched with oxygen-vacancy defects. The introduction of amorphous SeO_X not only generates abundant O_V sites and increases the electrochemically active surface area, but also induces pronounced interfacial charge redistribution and tunes the electronic structure of Ni centers. These changes weaken the overly strong chemisorption of reaction intermediates, establish a more favorable balance between adsorption and desorption, accelerate intermediate exchange on the NiOOH surface, and alleviate the strong *COOH affinity that limits UOR kinetics.[79]

At a more refined level of defect engineering, Ji *et al.* constructed a local microenvironment in Ni_3N by pairing electron-deficient N-vacancies (VN) with adjacent electron-rich Ni sites. Combined experiments and DFT calculations showed that the VN sites preferentially adsorb the N atom of urea, while the neighboring

View Article Online
DOI: 10.1039/D6CC01805J

Ni sites lower the formation barrier of NiOOH and promote its generation at lower potentials. This vacancy–metal-site pairing directs the UOR toward the NCO^- pathway, suppresses complete urea dissociation and excessive $NiOOH/Ni(OH)_2$ cycling, and thus reduces charge-transfer resistance and accelerates the overall reaction kinetics.[80] Beyond conventional defect engineering, composition-induced lattice strain in multicomponent alloys provides another effective means of regulating the local electronic environment. A representative example is the CuNiCo-7.8%Mo medium-entropy alloy reported by Wang *et al.*, in which Mo incorporation introduces a moderate local tensile lattice strain together with a built-in electric field. The resulting enhancement cannot be fully described by a simple d-band-center upshift. Instead, it is more directly reflected in optimized electron distribution, stronger urea adsorption, and faster interfacial charge transfer. *In situ* analyses further showed that this synergy favors a direct oxidation pathway before the Ni oxidation potential is reached, thereby lowering the required potential and improving UOR performance at large current densities.[86]

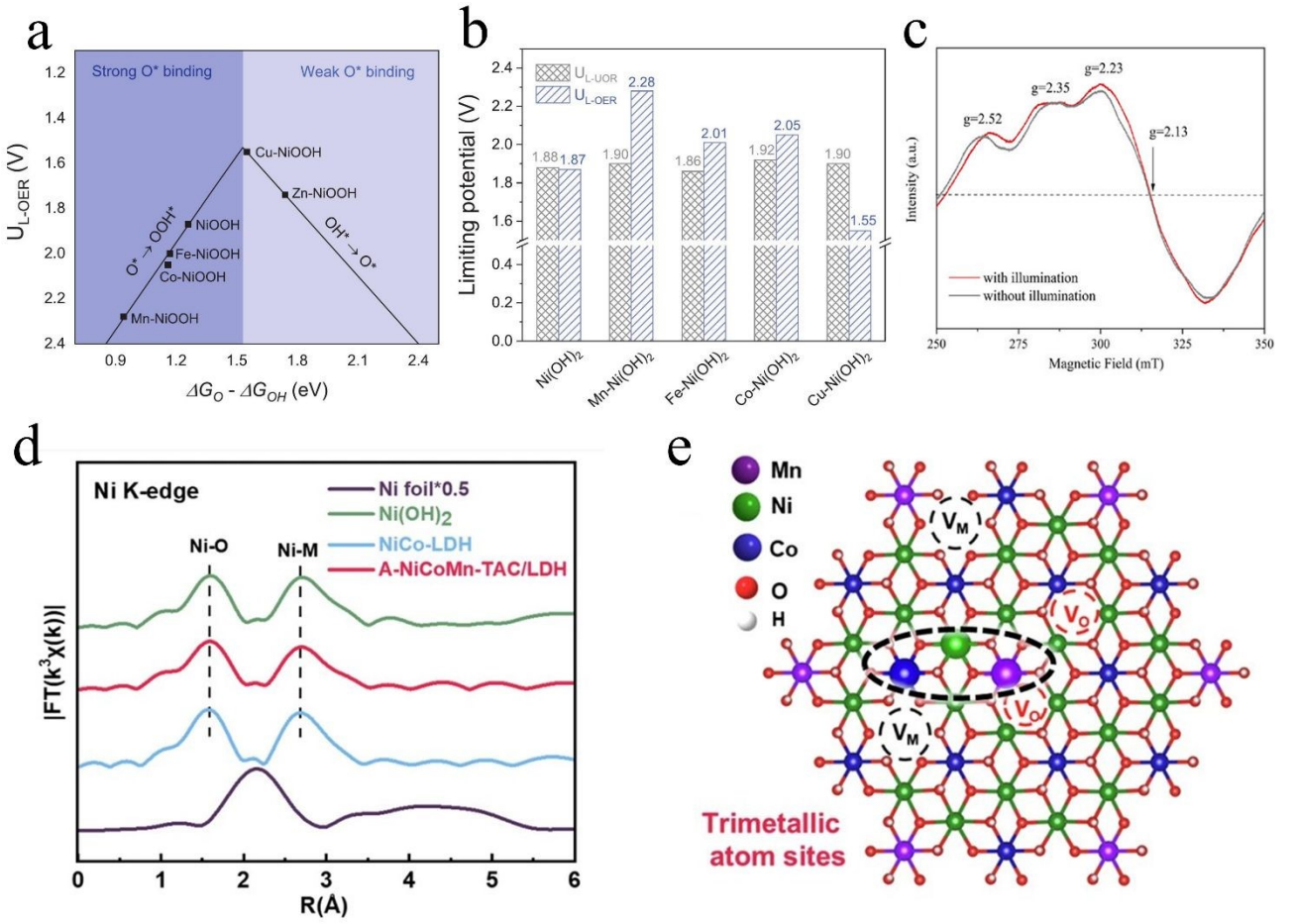

Fig. 8 a) Volcano plot of the OER limiting potential as a function of $\Delta G_O - \Delta G_{OH}$. b) Comparison of the theoretical limiting potentials for UOR and OER on undoped and doped β-NiOOH structures. Reproduced from ref. 78 with permission from Elsevier, Q. Jin, M. X. Garcia-Ortiz and L. Árnadóttir, J. Catal., 2026, 453, 116503, copyright 2026. c) Electron spin resonance (ESR) spectra of Mo-Ni_3S_2. Reproduced from ref. 10 with permission from John Wiley and Sons, Small, 2024, 20, 2403107, copyright 2024. d) FT-EXAFS fitting curves of NiCoMn-TAC/LDH in Ni R-space. e) Schematic diagram of the trimetallic atom sites structure with oxygen vacancies and metal defects of A-NiCoMn TAC/LDH. Reproduced from ref. 43 with permission from Springer Nature, Nat. Commun., 2025, 17, 213, copyright 2025.

4.3 Heterojunction Synergy and Built-in Electric Field

Constructing heterojunction interfaces to induce spontaneous electron transfer through Fermi-level differences, and thus generate a built-in electric field, has become a central strategy for directing interfacial charge transport. Guo *et al.* prepared two nickel sulfide heterojunctions with opposite electron-transfer directions, namely NiS/Ni_3S_2 (from Ni_3S_2 to NiS) and NiS/NiS_2 (from NiS to NiS_2). Experimental results and theoretical calculations showed that the NiS/Ni_3S_2 Mott–Schottky interface, because of its larger work-function difference, generates a stronger built-in electric field and a more continuous electron-transport pathway. This feature accelerates charge transfer and promotes the rapid *in situ* formation

View Article Online
DOI: 10.1039/D6CC01805J

of NiOOH active species. At the same time, electron depletion at the interfacial Ni_3S_2 region favors the adsorption of nucleophilic urea molecules and lowers the free-energy barrier of the key deprotonation step from $*CO(NH_2)_2$ to $*CON_2$ by stabilizing the carbonyl group. These results illustrate the importance of regulating the direction of interfacial electron transfer for optimizing UOR activity and selectivity.[87]

Interfacial charge redistribution also plays a key role in steering the adsorption of different functional groups in urea. Du *et al.* designed a $CoS_{1.097}/Ni_3S_2$ heterojunction in which spontaneous electron transfer from Ni_3S_2 to $CoS_{1.097}$ establishes a built-in electric field. DFT calculations showed that the resulting electrophilic Ni_3S_2 region preferentially interacts with the electron-withdrawing carbonyl group (C=O), whereas the nucleophilic $CoS_{1.097}$ region favors adsorption of the electron-donating amino group ($-NH_2$). This electrostatically driven interfacial adsorption mode promotes C-N bond cleavage and thereby accelerates urea decomposition.[88] Based on a similar principle of interfacial charge regulation, Yue *et al.* constructed a built-in electric-field-driven Ni_3Se_2@$NiMoO_4$/NF heterojunction catalyst. Spontaneous electron transfer from Ni_3Se_2 to $NiMoO_4$ produces an electrophilic, electron-deficient Ni_3Se_2 side and a nucleophilic, electron-rich $NiMoO_4$ side, enabling selective activation of the amino and carbonyl groups in urea. This complementary adsorption mode facilitates C-N bond dissociation and markedly lowers the free-energy barrier of this step, thereby accelerating urea decomposition (Fig. 9a, 9b).[45] In p–n heterojunction engineering, Liu *et al.* constructed an *in situ* grown NiCoP (n-type)/Co_3O_4 (p-type) composite electrocatalyst on nickel foam. Mott–Schottky analysis, together with XPS, UV–vis band-structure estimation, and DFT calculations, revealed interfacial band bending and spontaneous electron transfer, which together generate a built-in electric field. Combined with the 3D nanoflower-like architecture, this p–n interface optimizes the electronic structure, promotes charge transfer and urea conversion, and lowers the activation barrier for the UOR.[89]

From the perspective of structural design, Janus heterostructures provide a distinctive platform for interfacial synergy in multicomponent catalysts. Li *et al.* developed a carbophilicity-guided cooling crystallization strategy to synthesize RuNiW/W_2C Janus nanoparticles, in which the preferentially formed W_2C phase directs the growth of RuNiW during cooling. More importantly, the resulting Janus interface induces strong electronic interactions and charge redistribution, thereby regulating the valence state and d-band center of Ni, optimizing urea and intermediate adsorption, and lowering the UOR reaction barrier.[90]

Such heterointerfaces in multicomponent systems can effectively regulate the valence evolution of Ni sites and lower the barrier of key UOR steps. More importantly, rational interface engineering can also improve catalyst selectivity in complex media. Zhang *et al.* reported an Fe-doped Ni_3S_2@$NiSe_2$ heterojunction, in which Fe incorporation adjusts the local electronic structure and promotes surface reconstruction into Fe-NiOOH during the UOR. *In situ* Raman, *In situ* FTIR and DFT analyses showed that Fe facilitates the dehydrogenation of $*CONH_2NH$ and *CONHN intermediates, strengthens d–p hybridization, and promotes the conversion of the toxic *CO intermediate. At the same time, it facilitates CO_2 formation and lowers the barrier for CO_2 desorption. As a result, the catalyst effectively suppresses the competing OER and maintains high hydrogen-production efficiency and UOR selectivity even in actual human urine.[91]

4.4 Multi-scale Microenvironment Engineering

Merely optimizing the atomic-scale electronic structure, as discussed in Sections 4.1–4.3, is not sufficient to overcome the mass-transport limitations that arise at industrially relevant high current densities. For this reason, increasing attention has shifted toward reconstructing the catalytic microenvironment at the mesoscopic and macroscopic levels. With respect to the ionic microenvironment, Li *et al.* systematically investigated interfacial effects at the interface between the electrode and the electrolyte and showed that a dendritic $NiCoMoCuO_XH_Y$ catalyst generates a tip-discharge effect, which enhances the local electric field. This intensified field promotes the enrichment of OH^- within the electric double layer (EDL), thereby accelerating the dehydrogenation and oxidation steps of urea molecules.[92] Focusing on the coordination microenvironment, Kim *et al.* reported an accessible NiFe oxalate framework with prismatic nanostructures. XPS, XAS and DFT analyses showed that the electron-withdrawing oxalate ligands create electron-deficient Ni centers and favor O-bound adsorption of urea through its carbonyl oxygen, while Fe dopants increase the charge density of oxalate-O and strengthen its hydrogen-bond interaction with urea. This distinctive organic–inorganic coordination environment facilitates C-N bond cleavage, suppresses the over-oxidation of Ni at high potentials, and thereby reduces interference from the OER.[93]

Beyond regulation of the ionic and coordination microenvironment, interfacial bond-length engineering provides a more direct structural route for steering the UOR pathway. Guo *et al.* showed that elongating the Ni-Te bond in nickel telluride from 2.49 Å to 2.71 Å induces asymmetric charge redistribution and shifts the Ni d-band center farther away from the Fermi level. This sub-angstrom bond-length modulation promotes OH^- accumulation and the rapid formation of an active Ni^{3+}-O layer. At the same time, it stabilizes the $*H_2NCNO$ intermediate by strengthening its C-N bond, thereby favoring dehydrogenation toward N2 while suppressing C-N cleavage and NO_X^- formation (Fig. 9c).[48]

At high current densities, severe blockage of active sites by gas bubbles makes optimization of the macroscopic interfacial physical field equally important. This issue is not only an activity limitation but also a durability concern: persistent bubble adhesion, local OH^- and urea depletion, and increased interfacial resistance may promote current fluctuations, mechanical stress on reconstructed layers, and apparent performance decay. Therefore, in addition to improving intrinsic activity, the coupling among surface wettability, bubble-release behavior, and interfacial mass and electron transport is particularly critical for maintaining UOR operation under large-current conditions. Lei *et al. in situ* grew Fe-doped NiTe/$NiSe_2$ nanosheet arrays on nickel foam. The rough and open nanoarray structure promoted electrolyte infiltration and continuous electron

View Article Online
DOI: 10.1039/D6CC01895J

transport. Under vigorous gas evolution, dense and small bubbles detached rapidly from the electrode surface (Fig. 9d-h), in sharp contrast to the large bubbles that adhered to $NiTe/NiSe_2$. This superhydrophilic–superaerophobic micro- and nanostructured surface suppresses bubble accumulation, mitigates the formation of a dynamic gas barrier, reduces ohmic loss, and thus provides an effective macroscopic strategy for sustaining urea electrolysis at high current density.[46] To further improve macroscopic fluid transport, Liao *et al.* constructed a wood-derived integrated Ni/CW electrode using carbonized natural wood as a hierarchically porous scaffold. Its aligned low-tortuosity microchannels and multiscale porosity facilitate electrolyte permeation, ion transport, and the rapid release of gaseous products, while the mastoid-like Ni nanoparticles endow the surface with superhydrophilic and superaerophobic characteristics. This biomass-inspired architecture offers a low-cost and sustainable route for alleviating mass-transfer limitations, and serves as an important macroscopic complement to multiscale microenvironment engineering.[94]

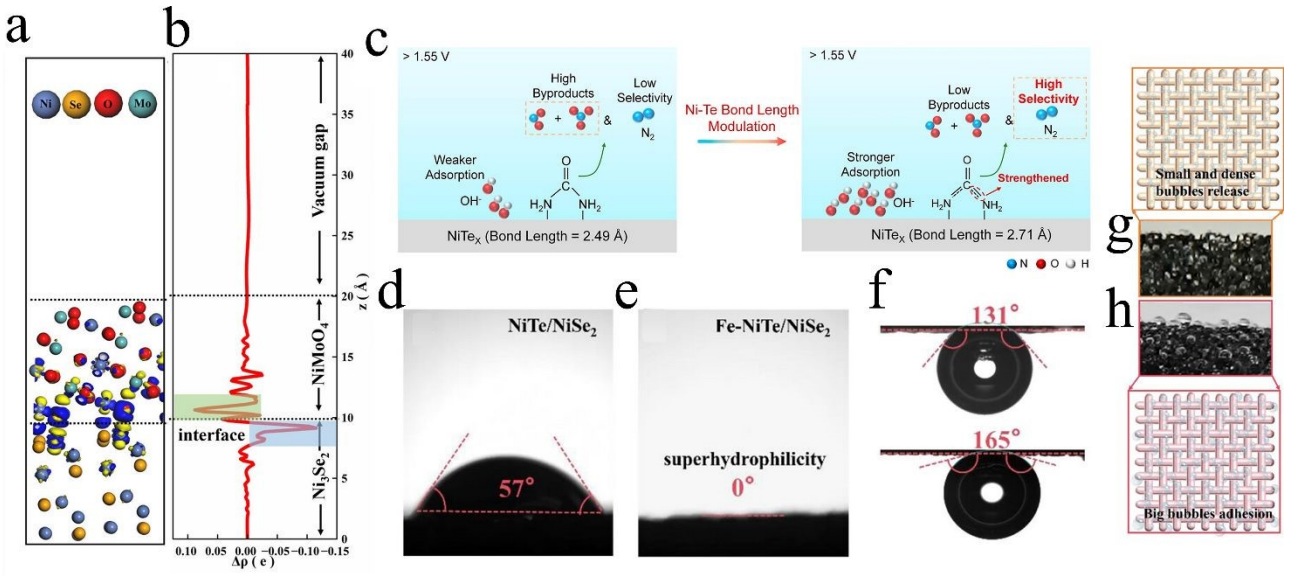

Fig. 9 Electronic structure analysis of Ni_3Se_2@$NiMoO_4$/NF heterojunction: a) Charge density difference distribution of Ni_3Se_2@$NiMoO_4$/NF (The blue and yellow isosurfaces represent regions of electron accumulation and depletion). b) Planar charge density along Z-axis. Reproduced from ref. 45 with permission from John Wiley and Sons, Adv. Funct. Mater., 2026, 36, e17125, copyright 2026. c) Schematic illustration depicts a strategy for modulating the bond length of the interface microenvironment to influence the reaction pathway of the UOR on nickel tellurides. Reproduced from ref. 48 with permission from American Chemical Society, ACS Nano, 2025, 19, 42389-42401, copyright 2025. The contact angle tests of d) $NiTe/NiSe_2$ and e) $Fe\text{-}NiTe/NiSe_2$. f) The underwater air contact angle on the $NiTe/NiSe_2$ (the upper side) and $Fe\text{-}NiTe/NiSe_2$ (the lower side). The illustration of bubble behaviors and the real generated bubbles under the current density of 100 mA cm^{-2} on the g) $Fe\text{-}NiTe/NiSe_2$ and h) $NiTe/NiSe_2$. Reproduced from ref. 46 with permission from John Wiley and Sons, Adv. Funct. Mater., 2026, 33, e27710, copyright 2026.

5. Advanced Characterization and Methodological Standardization

With the deepening of research on UOR electrocatalysts, traditional ex situ characterization techniques have become insufficient to capture the transient evolution of active sites and the complex transformation of intermediates during the reaction process. Recently, *in situ* spectroscopic techniques coupled with isotope tracing methods have provided molecular-level evidence for revealing authentic structure-activity relationships. Meanwhile, establishing rigorous quantitative detection standards for products is crucial to avoid false-positive results.

5.1 *In situ* Spectroscopy and Active Species Tracking

A molecular level understanding of urea adsorption under operating potentials is essential for clarifying the UOR mechanism. Using an electrodeposited Ni film as a model catalyst, An *et al.* performed *in situ* ATR-SEIRAS and, by combining ^{15}N-labeled urea experiments with polarization-resolved spectra, identified an O-terminally adsorbed $O{=}C(NH_2)_2$ species as the adsorption precursor. The absence of the 1573 cm^{-1} band in the s-polarized spectra further suggested that urea is vertically adsorbed on the Ni surface through the oxygen atom. As the potential increased, this oxygen-bound configuration gradually rotated and evolved into the N-terminal intermediate NH_2CONH_2, which then underwent dehydrogenation to generate CNO^-, CO_2, and N_2 (Fig. 10a, 10b). These results provide direct spectroscopic evidence that the adsorption configuration changes during the UOR on Ni-based catalysts.[41]

To follow the dynamic evolution of bimetallic active species, Yang *et al.* used *in situ* Raman spectroscopy to monitor the phase transformation of NiCo double hydroxides (DHs) during the UOR.

View Article Online
DOI: 10.1039/D6CC01805J

Spectra collected at different potentials showed that $Ni(OH)_2$ was oxidized to NiOOH, whereas the Co component first evolved into CoOOH and then further into high-valent CoO_2 under reaction conditions (Fig. 10c). These observations indicate that the catalytically relevant state is not a single-component phase, but a complex mixed phase composed of NiOOH, CoOOH, and CoO_2 that forms *in situ*. Raman peak shifts, together with electrochemical analysis, further showed that Co incorporation promotes earlier formation of NiOOH and induces elongation of the Ni–O bond as well as greater structural disorder, all of which are associated with enhanced UOR activity.[95]

For a more rigorous analysis of catalyst evolution under working conditions, the combination of *in situ* and ex situ synchrotron XAS can provide element-specific information at the atomic scale. Duan *et al.* tracked Mn-doped NiS_2 during the UOR and found that the Ni K-edge showed only a slight positive shift during short *in situ* measurements, whereas the fully activated catalyst displayed a clear structural transformation from Ni–S to Ni–O coordination. These results indicate that the sulfide acts as a precatalyst and is gradually reconstructed into Mn-NiOOH from the surface toward the interior under anodic polarization. More importantly, Mn doping promotes CO_2 desorption and accelerates regeneration of Ni^{3+} active sites, thereby improving both the activity and durability of the UOR.[96] By contrast, *in situ* XAS can also be used to exclude, rather than verify, specific phase-transition scenarios. In the case of nickel ferrocyanide, $Ni_2Fe(CN)_6$, Geng *et al.* found that the Ni and Fe K-edge positions remained essentially unchanged during the *in situ* UOR test and stayed close to their initial divalent states, with no spectroscopic evidence for NiOOH formation within the *operando* time window. Together with *in situ* Raman and infrared spectroscopy, these results support a two-stage dual-site mechanism that does not rely on NiOOH formation. In this pathway, Ni sites mediate the chemical conversion of urea to NH_3, while Fe sites catalyze the subsequent electrochemical oxidation of NH_3 to N_2 (Fig. 10d, 10e).[35] Ge *et al*. further combined *in situ* Raman spectroscopy with XAS to carry out multimodal characterization of three-dimensional nickel borate and graphene arrays, and revealed the key stabilizing role of nonmetallic boron in suppressing the reduction of high-valent Ni species.[75]

Even so, *in situ* and *operando* data must be interpreted with particular caution. In a recent Perspective, Prajapati *et al.* outlined a best-practice framework for electrocatalytic characterization that covers vibrational spectroscopy, including IR and Raman, XAS, electrochemical mass spectrometry, reactor design, and theoretical modeling. They emphasized that mechanistic assignments must rigorously rule out artifacts arising from mismatches between reactor configuration and mass transport conditions, bubble effects, and beam-induced perturbations. They also stressed the importance of proper controls, isotope labeling, comparisons with prior literature and DFT results, and concurrent measurements of activity and products, so as to avoid false positives and overly extended mechanistic interpretations. In addition, they argued that complementary multimodal analysis is essential for cross-validating active species and reaction pathways, thereby improving mechanistic reliability.[97] More broadly, Moyo *et al.* emphasized that in hybrid water electrolysis, where the oxidation of small organic molecules or biomass-derived substrates competes with the OER, real-time *in situ* techniques are indispensable for capturing transient intermediates, including adsorbed radicals and reactive oxygen species, and for disentangling the dynamic pathways that govern reaction selectivity and kinetics.[98]

5.2 Isotope Tracing

Quantitative isotope measurements provide a powerful means of identifying atom sources and probing kinetic bottlenecks associated with proton transfer in heterogeneous electrocatalysis. In their review, Lin *et al.* systematically summarized the principles and applications of isotope labeling and kinetic isotope effects (KIEs). They emphasized that isotope labeling is particularly useful for tracing the source of specific elements, whereas H/D KIE analysis can be used to determine whether proton transfer or proton-related bond cleavage contributes to the rate-determining step. Although this framework was developed in a broader electrocatalytic context rather than specifically for the UOR, it offers an important methodological basis for distinguishing pure electron-transfer pathways from proton coupled electron transfer (PCET) pathways in urea oxidation.[99]

In mechanistic studies involving lattice oxygen participation, isotope tracing can provide especially direct evidence. Zhang *et al.* carried out the UOR in an $H_2{}^{18}O$-labeled alkaline electrolyte and then analyzed the postreaction catalysts by SIMS depth profiling. The much higher $^{18}O/^{16}O$ ratio retained in NiClO-D than in NiOH-D, together with *in situ* FTIR evidence for faster CO_2 generation, supports a lattice-oxygen-involved pathway on high-valent Ni^{4+} sites rather than the conventional pathway on Ni^{3+} sites. These results indicate that lattice oxygen from the catalyst participates in the oxidation of carbon-containing intermediates toward CO_2 formation, while oxygen from the electrolyte replenishes the oxygen vacancies generated at the catalyst surface.[36]

In the context of wastewater treatment, Zhou *et al.* demonstrated the value of ^{15}N, ^{13}C, and ^{18}O isotope labeling for tracing the degradation pathways of chemical pollutants.[100] Although their discussion was not specifically centered on the UOR, the same methodological logic can be extended to urea oxidation. For example, ^{15}N-labeled urea, combined with isotopologue analysis of evolved N_2, could help determine whether the product originates from coupling between the two nitrogen atoms derived from one urea molecule or from cross-reactions with other nitrogen species in the electrolyte, thereby reducing false-positive mechanistic assignments. Ge *et al.* further pointed out that *in situ* differential electrochemical mass spectrometry (DEMS), especially when combined with isotope labeling, is a powerful tool for tracking gaseous products during the UOR. By resolving the isotopic distribution of evolved N_2 in real time, DEMS can directly distinguish intramolecular N–N coupling from intermolecular pathways. Even so, it should not be used as the sole criterion for selectivity evaluation. A more complete assessment of gaseous and liquid products, as well as overall catalytic selectivity, still requires complementary analyses such as gas chromatography (GC), ion chromatography (IC), and nuclear magnetic resonance (NMR) (Fig. 10f).[101]

View Article Online
DOI: 10.1039/D6CC01805J

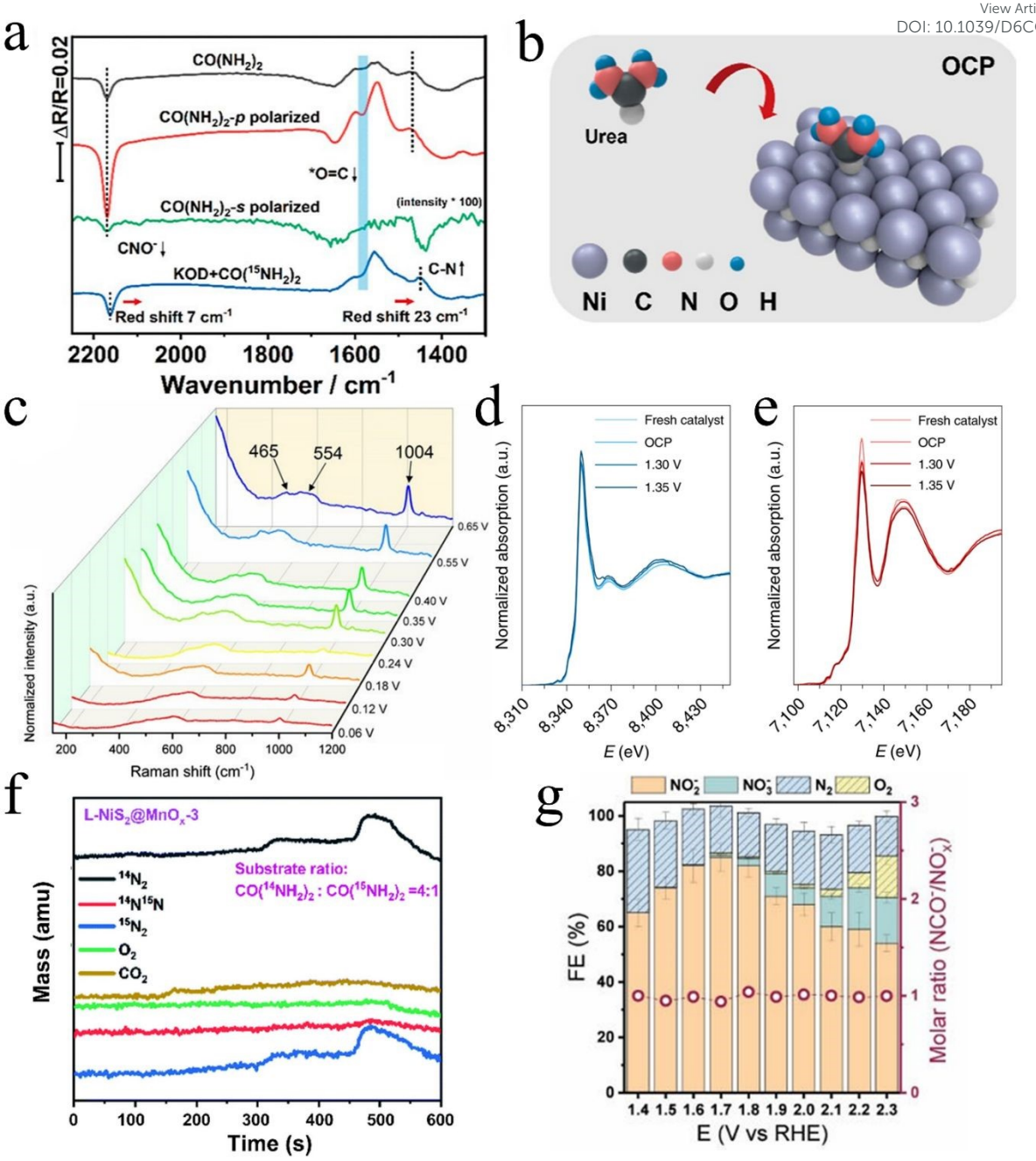

Fig. 10 a) Spectrum at 1.7 V (reference potential 0.9 V) in the range of 2250−1350 cm $^{-1}$, which was collected under regular light (gray line), p-polarized light (red line), s-polarized light (green line), and KOD + $CO(^{15}NH_2)_2$ (blue line). b) Schematic representation structure for an absorbed urea on a Ni film catalyst in an alkaline solution at OCP (Open Circuit Potential). Reproduced from ref. 41 with permission from American Chemical Society, J. Phys. Chem. C, 2023, 128, 77-84, copyright 2023. c) *In situ* Raman spectra collected for $Ni_{0.2}Co_{0.8}$ DHs deposited on a roughened Au substrate as a function of potential versus Hg/HgO in 1M KOH+0.33M urea. Reproduced from ref. 95 with permission from John Wiley and Sons, Energy Technol., 2022, 10, 2101010, copyright 2022. (d, e) Ni (d) and Fe (e) K-edge X-ray absorption near-edge structure (XANES) spectra showing the $Ni_2Fe(CN)_6$ catalyst under different conditions. Reproduced from ref. 35 with permission from Springer Nature, Nat. Energy, 2021, 6, 904-912, copyright 2021. f) *In situ* electrochemical mass spectrometry isotope tracing experiments under the catalysis of L-NiS_2@MnO_X in 1 M KOH + 0.33 M urea ($CO(^{15}NH_2)_2$: $CO(NH_2)_2$ ≈ 4:1). Reproduced from ref. 101 with permission from Elsevier, Surf. Interfaces, 2023, 41, 103230, copyright 2023. g) FEs of major products of short-term 1 h urea electrolysis and [NCO^- : NO_X^-] (x=1, 2) molar ratio as a function of the applied potential. Reproduced from ref. 33 with permission from John Wiley and Sons, Angew. Chem. Int. Ed., 2022, 61, e202209839, copyright 2022.

View Article Online
DOI: 10.1039/D6CC01805F

5.3 Standardized Quantification and Stability Evaluation Protocols

Despite the rapid progress in UOR research, accurate quantification of urea conversion products remains challenging. Tatarchuk *et al.* showed clearly that nickel-catalyzed UOR does not proceed as a single six-electron pathway leading exclusively to N_2. Instead, it follows a complex network of competing routes, in which nitrite is often the dominant product and cyanate is generated in a nearly stoichiometric ratio to NO_X^- over a broad potential range (Fig. 10g). By combining in-line gas chromatography, ion chromatography, and nuclear magnetic resonance, they demonstrated that rigorous multimodal product analysis is essential for correctly resolving UOR selectivity and for avoiding the oversimplified assumption that N_2 is the sole product.[33]

To improve the reliability of low-concentration urea quantification, Li *et al*. systematically compared the methods commonly used in photocatalysis and electrocatalysis. They found that indirect assays, such as the diacetylmonoxime-thiosemicarbazide (DAMO-TSC) method and the urease method, can introduce substantial deviations in complex reaction media. In particular, the DAMO-TSC method is poorly suited to systems containing NO_2^-. On this basis, they proposed a rigorous quantification protocol that emphasizes choosing the analytical method according to the specific reaction conditions, mandatory verification with a more direct technique such as ^{1}H nuclear magnetic resonance (^{1}H-NMR) or high-performance liquid chromatography (HPLC), and the use of isotope-tracing experiments when needed. Although this framework was developed for photo(electro)catalytic urea synthesis rather than the UOR, its transfer to UOR quantification should be treated with caution. The two systems differ in reaction direction and analytical matrix: urea is typically the low-concentration target product in synthesis studies, whereas in UOR it is the consumed substrate and coexists with strongly alkaline electrolyte, anodically generated NO_2^-/NO_3^- and NCO^- species, and gaseous products. Therefore, the transferable value of the framework shown in Fig. 11 is better interpreted as its analytical logic-matrix-dependent method selection, matrix-matched calibration and interference tests, cross-validation by ^{1}H-NMR or HPLC, and isotope tracing when product assignment is ambiguous-rather than as a UOR-specific quantification procedure. For UOR, this logic should be integrated with product-oriented analyses, such as IC for NO_2^-/NO_3^-/NCO^- and GC/DEMS for gaseous products, to establish a more reliable mass- and charge-balanced selectivity evaluation.[33,52,101]

Beyond product and substrate quantification, rigorous standardization should also include catalyst stability evaluation under practically relevant current densities, together with electrolyte-side and post-reaction analyses that help distinguish intrinsic active-phase degradation from component leaching and transport-induced apparent decay.[46,52] Zhang *et al.* combined *in situ* spectroscopic characterization with electrolyte analysis to study $NiCoVO_X$. Their results showed that high-valent V sites act as additional OH^- adsorption centers, promote rapid regeneration of Ni active sites during the UOR, and suppress excessive accumulation of NiOOH. More importantly, inductively coupled plasma mass spectrometry (ICP-MS) revealed that the dissolved V concentration after the UOR was only 2.1 ppm, corresponding to 19% leaching, whereas after the OER it reached 10.5 ppm, corresponding to 97% leaching. These results suggest that quantitative monitoring of dissolved metal species should be incorporated into standardized durability assessment, because electrolyte-side leaching analysis is necessary for accurately evaluating true catalyst stability and activity retention.[54]

6. Conclusions and Future Perspectives

6.1 Summary

This review summarizes recent advances in nickel-based electrocatalytic materials for the urea oxidation reaction (UOR), with particular emphasis on the relationships between catalyst structure and catalytic behavior, from microscopic reaction pathways to interfacial regulation across multiple scales. As a promising anodic half-reaction to replace the oxygen evolution reaction, the UOR offers clear dual benefits: it can lower the energy consumption of hydrogen production during water electrolysis, while also enabling the resource-oriented treatment of nitrogen-containing wastewater. With regard to reaction pathways, current understanding has moved from macroscopic phenomenological descriptions toward atomic-level insight. The traditional indirect oxidation mechanism is no longer the only explanatory framework. Direct oxidation pathways based on high-valence metal sites, including Ni^{3+} and Ni^{4+}, as well as the lattice oxygen mechanism, in which lattice oxygen participates in the reaction, are now recognized as effective routes for lowering reaction barriers. In particular, the recently identified two-step pathway involving ammonia intermediates, together with dual-site synergistic mechanisms, provides a new physicochemical basis for overcoming the linear scaling relations associated with intermediate adsorption. These advances also clarify the important role of nontraditional pathways in improving catalytic efficiency.

In terms of catalytic regulation, kinetic limitations have been addressed through multilevel strategies that range from atomic-scale electronic structure tuning to macroscopic physical field engineering. At the atomic level, spin-state regulation and defect engineering can precisely optimize the adsorption energies of key intermediates, such as *NCO. At the mesoscale, built-in electric field engineering in heterojunctions promotes directional charge transport and spatially differentiated adsorption of substrate molecules. At the macroscale, microenvironment reconstruction, including ion enrichment and the construction of superaerophobic interfaces, helps alleviate mass-transfer limitations under industrially relevant high-current conditions. In addition, the combination of advanced *in situ* spectroscopic techniques with standardized quantitative protocols provides solid methodological support for mechanistic verification and reliable performance evaluation.

View Article Online
DOI: 10.1039/D6CC01805J

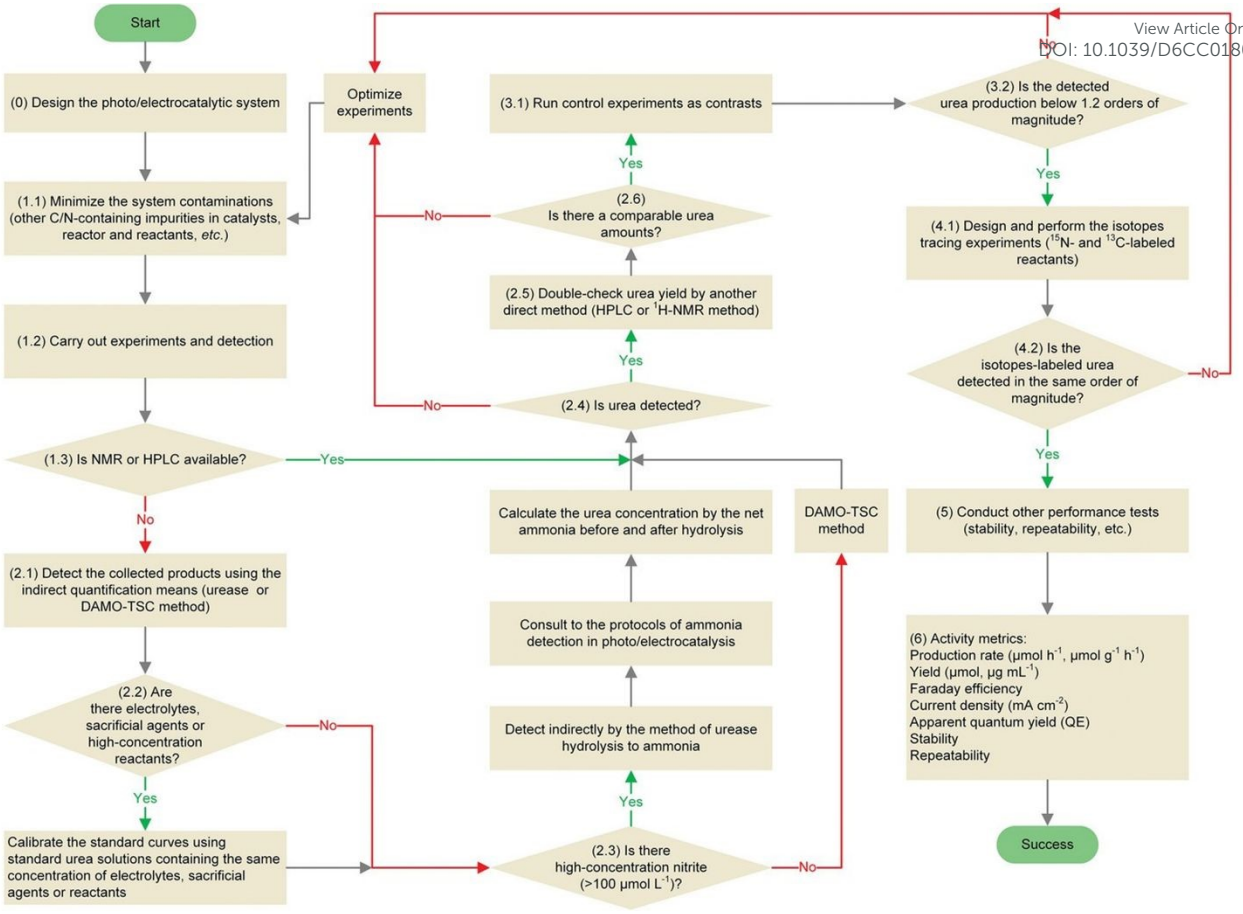

Fig. 11 Representative quantification framework originally proposed for photo/electrocatalytic urea synthesis. In the UOR context, this framework should be regarded as a transferable analytical reference for matrix-dependent urea quantification and cross-validation, rather than as a complete UOR-specific product-analysis protocol. Reproduced from ref. 52 with permission from John Wiley and Sons , Small Methods, 2022, 6, 2200561, copyright 2022.

6.2 Challenges and Future Perspectives

While nickel-based UOR catalysts have shown clear promise for lowering the energy consumption of electrolysis and enabling wastewater remediation, moving from laboratory proof-of-concept to industrial application still requires major advances in mechanistic understanding and in adaptation to realistic operating conditions. In particular, *in situ* elucidation of reaction kinetics across full spatiotemporal scales is essential for guiding rational catalyst design. Most current mechanistic models still rely mainly on spectroscopic detection of steady-state intermediates, such as *NCO. By contrast, quantitative approaches for capturing short-lived transient species and tracking the dynamic behavior of lattice oxygen remain highly limited. Future work should therefore give priority to transient spectroscopic techniques with ultrahigh femtosecond or picosecond time resolution, including transient absorption spectroscopy and time-resolved Raman spectroscopy.

By following reaction kinetics *in situ*, such methods could enable more precise identification of the dynamic evolution of metastable intermediates, such as *NH radicals. This level of kinetic understanding is critical for designing catalytic interfaces that can overcome the rate-determining step (RDS) and promote efficient N-N coupling. Such targeted interface design is expected to further improve the selective conversion of urea into clean products, particularly N_2. At the same time, the combination of isotope labeling with online differential electrochemical mass spectrometry is also needed. This approach could help establish quantitative relationships between the lattice oxygen mechanism and structural stability, while clarifying the intrinsic role of high-valent Ni^{4+} species in the competing kinetics of C-N bond cleavage and O-O bond formation.

Theoretical simulation also needs to move closer to realistic reaction environments. In particular, more accurate explicit solvation models and constant-potential methods should be incorporated to describe proton coupled electron transfer processes in the electric double layer more faithfully, thereby narrowing the gap between theoretical prediction and experimental observation.

Alongside these mechanistic issues, catalyst adaptability in complex real-world environments must also be addressed. Beyond chloride-rich urine, practical wastewater matrices may also contain organic constituents, hardness ions, competing anions, and, in industrial or mixed streams, heavy-metal ions. These species may adsorb on or precipitate near reconstructed NiOOH layers, modify local pH and OH^-/urea availability, compete with urea for interfacial

View Article Online
DOI: 10.1039/D6CC01805J

sites, or participate in side redox chemistry, thereby affecting both active-phase reconstruction and long-term N_2 selectivity. Future evaluations should therefore combine matrix-matched synthetic and real effluents with operando tracking of NiOOH reconstruction, electrolyte-side metal-leaching analysis, and mass- and charge-balanced quantification of N_2, NO_2^-/NO_3^-, NCO^-, and residual urea. On this basis, interfacial microenvironments with ion-sieving and anti-fouling capability, for example through electrostatic repulsion or Lewis acid-base interactions, may help suppress catalyst poisoning, chloride corrosion, and toxic byproduct formation. For industrial deployment, research also needs to move beyond static material design toward dynamic self-repair strategies and system-level integration. By understanding how active sites can be regenerated *in situ* during operation, it should be possible to develop catalysts that better withstand structural evolution and bubble impact under ampere-level currents, and thereby support the efficient integration of membraneless electrolyzers and direct urea fuel cells. Ultimately, only through deeper understanding of transient reaction kinetics and coordinated optimization of interfacial stability across multiple scales can nickel-based UOR technology become a practically important component of a clean hydrogen economy.

Author contributions

Riyi Zhang conducted the comprehensive literature survey and drafted the sections on mechanistic insights into the urea oxidation reaction(UOR), dynamic reconstruction and active-site evolution, interfacial regulation strategies, and advanced characterization and methodological standardization. Yong Yan collected the background literature on the UOR and contributed to the writing of the Introduction. Zhihao Yi contributed to the writing of the Challenges and Future Perspectives section. Yong Yan, Dong Wang, and Zhihao Yin contributed to the conceptualization, editing, and overall refinement of the manuscript. All authors reviewed and approved the final manuscript.

Conflicts of interest

There are no conflicts to declare.

Acknowledgements

This work was supported by the National Natural Science Foundation of China (Nos. 22278012, 21936001, and 22176230).The authors gratefully acknowledge the academic support and stimulating research environment provided by Beijing University of Technology, TU Ilmenau, and the State Key Laboratory of Chemistry for NBC Hazards Protection during the preparation of this review.

Data availability

No primary research results, software or code have been included and no new data were generated or analysed as part of this review.

References

1. X. Gao, P. Wang, X. Sun, M. Jaroniec, Y. Zheng and S. Z. Qiao, *Angew. Chem. Int. Ed.*, 2025, **64**, e202417987.
2. J. Li, Y. Ma, X. Mu, X. Wang, Y. Li, H. Ma and Z. Guo, *Adv. Sci.*, 2025, **12**, 2411964.
3. K. Kawashima, R. A. Márquez, Y. J. Son, C. Guo, R. R. Vaidyula, L. A. Smith, C. E. Chukwuneke and C. B. Mullins, *ACS Catal.*, 2023, **13**, 1893-1898.
4. P. Wang, X. Gao, M. Zheng, M. Jaroniec, Y. Zheng and S. Z. Qiao, *Nat. Commun.*, 2025, **16**, 2424.
5. G. Zhan, L. Hu, H. Li, J. Dai, L. Zhao, Q. Zheng, X. Zou, Y. Shi, J. Wang, W. Hou, Y. Yao and L. Zhang, *Nat. Commun.*, 2024, **15**, 5918.
6. N. Q. Tran, N. H. Vu, J. Yu, K. V. P. Nguyen, T. T. N. Tran, T.-K. Truong, L. Peng, T. A. Le and Y. Kawazoe, *J. Energy Chem.*, 2024, **97**, 687-699.
7. A. Vignesh, G. Gnana kumar, P. Vajeeston and A. Manthiram, *Adv. Energy Mater.*, 2025, **15**, 2405025.
8. X. Gao, J. Hu, S. Zhang, P. Wang, Z. Wang, P. Chen, Y. Zheng and S. Z. Qiao, *Adv. Mater.*, 2026, **38**, e21945.
9. L. Cai, H. Bai, J. Li, F. Xie, K. Jiang, Y.-R. Lu, H. Pan and Y. Tan, *Energy Environ. Sci.*, 2025, **18**, 2415-2425.
10. P. Wang, W. Zheng, Y. Qu, N. Duan, Y. Yang, D. Wang, H. Wang and Q. Chen, *Small*, 2024, **20**, 2403107.
11. X. Ning, W. Chen, Y. Wu, Q. Zang, S. Yuan, J. Li, Z. Xu and Y. Wang, *J. Environ. Chem. Eng.*, 2025, **13**, 118646.
12. Y. Hu, L. Shao, Z. Jiang, L. Shi, Q. Li, K. Shu, H. Chen, G. Li, Y. Dong, T. Wang, J. Li, L. Jiao and Y. Deng, *Adv. Funct. Mater.*, 2024, **34**, 2411011.
13. Z. Shi, Y. Zhang, W. Guo, Z. Niu, Y. Chen and J. Huang, *Adv. Funct. Mater.*, 2025, **35**, 2414935.
14. B. Lu, C. Lv, Y. Xie, L. Gao, J. Yan, K. Zhu, G. Wang, D. Cao and K. Ye, *Small*, 2023, **19**, 2302923.
15. S. Xu, X. Ruan, M. Ganesan, J. Wu, S. K. Ravi and X. Cui, *Adv. Funct. Mater.*, 2024, **34**, 2313309.
16. M. Zhong, J. Yang, M. Xu, S. Ren, X. Chen, C. Wang, M. Gao and X. Lu, *Small*, 2024, **20**, 2304782.
17. V. Maheskumar, A. Min, C. J. Moon, R. A. Senthil and M. Y. Choi, *Small Struct.*, 2023, **4**, 2300212.
18. K. Yang, L. Hao, Y. Hou, J. Zhang and J.-H. Yang, *Int. J. Hydrogen Energy*, 2024, **51**, 966-981.
19. S. Ghosh, D. Bagchi, I. Mondal, T. Sontheimer, R. V. Jagadeesh and P. W. Menezes, *Adv. Energy Mater.*, 2024, **14**, 2400696.
20. M. Safeer N. K, C. Alex, R. Jana, A. Datta and N. S. John, *J. Mater. Chem. A*, 2022, **10**, 4209-4221.

21. M. S. Naduvil Kovilakath, C. Alex, N. N. Rao, D. Bagchi, A. Tayal, S. C. Peter and N. S. John, *Chem. Mater.*, 2024, **36**, 5343-5355.
22. J. Wan, Z. Wu, G. Fang, J. Xian, J. Dai, J. Guo, Q. Li, Y. You, K. Liu, H. Yu, W. Xu, H. Jiang, M. Xia and H. Jin, *J. Energy Chem.*, 2024, **91**, 226-235.
23. M. Liu, W. Zou, S. Qiu, N. Su, J. Cong and L. Hou, *Adv. Funct. Mater.*, 2023, **34**, 2310155.
24. K. Ge, Y. Geng, Y. Zhao, Z. Wang, J. Wang, Y. Guo, M. Yang, H. Cui, Y. Hu, B. Shen and Y. Yang, *Adv. Funct. Mater.*, 2025, **35**, 2505346.
25. Z. Zhu, K. Ge, Z. Li, J. Hu, P. Chen and H. Bi, *Small*, 2023, **19**, 2205234.
26. A. Sohel, M. S. N. Kovilakath, P. J. Gogoi, H. Ansari, P. Phukan, S. Bag, N. S. John and A. Baksi, *Small*, 2024, **20**, 2405160.
27. D. Zhu, H. Zhang, J. Miao, F. Hu, L. Wang, Y. Tang, M. Qiao and C. Guo, *J. Mater. Chem. A*, 2022, **10**, 3296-3313.
28. A. K. Satheesan, R. Madhu, S. Nagappan, H. N. Dhandapani, A. De, S. Singha Roy, P. Mazumder and S. Kundu, *Chem. Commun.*, 2025, **61**, 4092-4109.
29. W. Jiang, J. Zhang, J. Wu, Z. Zhai, T. Yu, L. Luo and S. Yin, *Adv. Energy Mater.*, 2025, **16**, e03978.
30. X. Gao, X. Bai, P. Wang, Y. Jiao, K. Davey, Y. Zheng and S. Z. Qiao, *Nat. Commun.*, 2023, **14**, 5842.
31. P. Qiao, G. Li, X. Xu, D. Wang, F. Wang, L. Xu, L. Lu, H. Cong and M. Sun, *Adv. Funct. Mater.*, 2025, **35**, 2421136.
32. D. Li, X. Zhou, Q. Ruan, L. Liu, J. Liu, B. Wang, Y. Wang, X. Zhang, R. Chen, H. Ni, C. Huang, H. Wang and P. K. Chu, *Adv. Funct. Mater.*, 2024, **34**, 2313680.
33. S. W. Tatarchuk, J. J. Medvedev, F. Li, Y. Tobolovskaya and A. Klinkova, *Angew. Chem. Int. Ed.*, 2022, **61**, e202209839.
34. N. N. Rao, C. Alex, M. Mukherjee, S. Roy, A. Tayal, A. Datta and N. S. John, *ACS Catal.*, 2024, **14**, 981-993.
35. S.-K. Geng, Y. Zheng, S.-Q. Li, H. Su, X. Zhao, J. Hu, H.-B. Shu, M. Jaroniec, P. Chen, Q.-H. Liu and S.-Z. Qiao, *Nat. Energy*, 2021, **6**, 904-912.
36. L. Zhang, L. Wang, H. Lin, Y. Liu, J. Ye, Y. Wen, A. Chen, L. Wang, F. Ni, Z. Zhou, S. Sun, Y. Li, B. Zhang and H. Peng, *Angew. Chem. Int. Ed.*, 2019, **58**, 16820-16825.
37. K. Dang, L. Wu, S. Liu, S. Zhao, Y. Zhang and J. Zhao, *Angew. Chem. Int. Ed.*, 2025, **64**, e202423457.
38. H. Zhang, Y. Bai, X. Lu, L. Wang, Y. Zou, Y. Tang and D. Zhu, *Inorg. Chem.*, 2023, **62**, 5023-5031.
39. W. Li, X. Lu and Z. Li, *Adv. Energy Mater.*, 2026, **16**, e04716.
40. B. Suzhen, Z. Yi, T. Zhengshan, C. Kesheng, L. Xingwu and W. Haoqi, *Prog. Chem.*, 2025, **37**, 1769-1791.
41. Z.-C. An, G. Li, L.-F. Ji, M.-W. Lin, R. Huang, B.-W. Zhang, Y.-X. Jiang and S.-G. Sun, *J. Phys. Chem. C*, 2023, **128**, 77-84.
42. L. Fei, C. Li, H. Sun, Z. Wei, Z. Wei, Y. Li, Y. Gu, I. V. Alexandrov, A. S. Kvyatkovskaya, M. Xu, R. Ran and W. Zhou, *Energy Fuels*, 2025, **39**, 12235-12243.
43. T. Li, Y. Hu, Z. Sun, M. Sun, B. Huang, W. Chen and B. Liu, *Nat. Commun.*, 2025, **17**, 213.
44. L. Hou, C. Sun, Z. Zhang, H. Jang, Z. Li, M. G. Kim, J. Cho, S. Liu and X. Liu, *Adv. Funct. Mater.*, 2025, **36**, e19865.
45. Y. Yue, Y. Wang, N. Jian, S. Liu, Z. Wang, H. Li, H. Zhao and W. Cai, *Adv. Funct. Mater.*, 2026, **36**, e17125.
46. M. Lei, Y. Zhao, X. Sun, Y. Pan, Y. Liu, J. Kang, D. Wei, L. Zou and Y. Pei, *Adv. Funct. Mater.*, 2026, **33**, e27710
47. X. Qiang, Y. Yao, J. Yin, P. Da, Z. Mu, K. Shen, Y. Sun, Y. Zhang, P. Li, Z. Li, P. Xi and C. H. Yan, *Angew. Chem. Int. Ed.*, 2025, **64**, e202424014.
48. P. Guo, S. Cao, W. Chen, W. Huang, X. Lu, Y. Zhang, Y. Wang, P. Zhang, R. Zou, S. Liu and X. Li, *ACS Nano*, 2025, **19**, 42389-42401.
49. H. Sun, Z. Luo, M. Chen, T. Zhou, B. Wang, B. Xiao, Q. Lu, B. Zi, K. Zhao, X. Zhang, J. Zhao, T. He, J. Zhang, H. Cui, F. Liu, C. Wang, D. Wang and Q. Liu, *ACS Nano*, 2024, **18**, 35654-35670.
50. T. Li, Z. Zheng, Z. Chen, M. Zhang, Z. Liu, H. Chen, X. Xiao, S. Wang, H. Qu, Q. Fu, L. Liu, M. Zhou, B. Wang and G. Zhou, *Energy Environ. Sci.*, 2025, **18**, 4996-5008.
51. L. Chen, L. Wang, J. T. Ren, H. Y. Wang, W. W. Tian, M. L. Sun and Z. Y. Yuan, *Small Methods*, 2024, **8**, 2400108.
52. D. Li, N. Xu, Y. Zhao, C. Zhou, L. P. Zhang, L. Z. Wu and T. Zhang, *Small Methods*, 2022, **6**, 2200561.
53. R. N. Durr, P. Maltoni, H. Tian, B. Jousselme, L. Hammarstrom and T. Edvinsson, *ACS Nano*, 2021, **15**, 13504-13515.
54. J. Zhang, P. Wang, M. Zheng, R. K. Hocking, Y. Zheng and S.-Z. Qiao, *ACS Catal.*, 2025, **15**, 3143-3152.
55. V. Vedharathinam and G. G. Botte, *Electrochim. Acta*, 2013, **108**, 660-665.
56. W. Wen, Z. Fu, M. Zhao, N. Gao, Q. Yan, L. Qiang, S. He, Z. Wang, L. Shi, H. Xiao and J. Jia, *J. Alloys Compd.*, 2025, **1042**, 184013.
57. P. Wang, X. Bai, H. Jin, X. Gao, K. Davey, Y. Zheng, Y. Jiao and S. Z. Qiao, *Adv. Funct. Mater.*, 2023, **33**, 2300687.
58. Z. Shen, Y. Qi, W. Ge, H. Jiang and C. Li, *Ind. Eng. Chem. Res.*, 2023, **62**, 8736-8743.
59. V. M. Zemtsova, A. G. Oshchepkov and E. R. Savinova, *ACS Catal.*, 2023, **13**, 13466-13473.
60. Y. Yang, J. A. Yuwono, T. Whittaker, M. M. Ibanez, B. Wang, C. Kim, A. Y. Borisevich, S. Chua, J. P. Prada, X. Wang, P. O. Autran, R. R. Unocic, L. Dai, A. Holewinski and N. M. Bedford, *Adv. Mater.*, 2024, **36**, 2403187.
61. G. Hopsort, E. Piguet, L. Latapie, K. Groenen Serrano, K. Loubière and T. Tzedakis, *Electrochim. Acta*, 2024, **479**, 143886.
62. L. Yang, W. Hu, Z. Chang, T. Liu, D. Fang, P. Shao, H. Shi and X. Luo, *Environ. Int.*, 2021, **152**, 106512.
63. C. Yin, S. Wang, F. Yang and L. Feng, *J. Energy Chem.*, 2025, **106**, 340-350.
64. Y. Feng, N. Ran, X. Wang, Q. Liu, J. Wang, L. Liu, K. Suenaga, W. Zhong, R. Ma and J. Liu, *Adv. Energy Mater.*, 2023, **13**, 2302452.
65. Q. Chen, X. Deng, H. He, L. Jiang, C. Liang, J. Zhang, R. Wang and J. Chen, *Chem. Eng. J.*, 2024, **484**, 149561.
66. Y. Chen, J. Meng, M. Xu, L. Qiao, D. Liu, Y. Kong, X. Hu, Q. Liu, M. Chen, S. Lyu, R. Tong and H. Pan, *Adv. Funct. Mater.*, 2025, **35**, 2413474.
67. K. Wu, W. Chen, S. Zhu, H. Liu, D. Wen, R. Zou and B. Zhu, *Adv. Funct. Mater.*, 2025, **36**, e20435.
68. Y. Zhu, C. Liu, S. Cui, Z. Lu, J. Ye, Y. Wen, W. Shi, X. Huang, L. Xue, J. Bian, Y. Li, Y. Xu and B. Zhang, *Adv. Mater.*, 2023, **35**, 2301549.
69. W. Bao, M. Yang, T. Ai, J. Han, Z. Deng, X. Zou, P. Jiang and J. Zhang, *Inorg. Chem. Front.*, 2024, **11**, 8824-8836.
70. J. Chen, H. Chen, H. Yin, H. He, Z. Wang, D. Yu, J. Liang, Y. Huang, L. Qin and D. Chen, *Chem. Eng. J.*, 2023, **477**, 146885.
71. Y. Bai, J. Li, L. Wang, J. Mu and Z. Feng, *Chem. Eng. J.*, 2025, **518**, 164468.
72. Y. Wang, L. Liang, Y. Tang, W. Xiao, T. Zhou, P. Shen and P. Tsiakaras, *Chem. Eng. J.*, 2025, **520**, 165516.
73. F. Yang, X. Huang, R. Li, S. Wang and L. Feng, *J. Phys. Chem. C*, 2024, **128**, 19436-19444.
74. K. Wang, M. Pei, Y. Shuai, Y. Liu, S. Deng, Z. Zhuang, K. Sun, W. Yan and J. Zhang, *ACS Energy Lett.*, 2024, **9**, 4682-4690.

View Article Online
DOI: 10.1039/D6CC01805J

75. J. Ge, J. Qi, Z. Liu and C. Yang, *Surf. Interfaces*, 2025, **76**, 107984.
76. X. Zhang, S. Feizpoor, M. Humayun and C. Wang, *Chem. Catalysis*, 2024, **4**, 100840.
77. W. K. Han, J. X. Wei, K. Xiao, T. Ouyang, X. Peng, S. Zhao and Z. Q. Liu, *Angew. Chem. Int. Ed.*, 2022, **61**, e202206050.
78. Q. Jin, M. X. Garcia-Ortiz and L. Árnadóttir, *J. Catal.*, 2025, **453**, 116503.
79. Q. Chen, J. Chen, X. Dong, C. Dong, Y. Zhou, J. Zhang, G. Wang and R. Wang, *Small*, 2025, **21**, 2409306.
80. C. Ji, H. Duan, C. Wang, G. Liang, X. Long, X. She, R. Zhang, F. Gong, D. Li, D. Yang and J. Liu, *Adv. Mater.*, 2025, **37**, 2503879.
81. X. Zheng, Y. Mei, Y. Zeng, Q. Hua and S. Lu, *Ind. Chem. Mater.*, 2026, DOI: 10.1039/D5IM00252D.
82. D. Liu, X. Guo, T. Yang, A. Kong, D. Lv, Y. Yang, X. Cui and R. Liu, *Adv. Funct. Mater.*, 2025, **36**, e17562.
83. Y. Zhou, Y. Wang, D. Kong, Q. Zhao, L. Zhao, J. Zhang, X. Chen, Y. Li, Y. Xu and C. Meng, *Adv. Funct. Mater.*, 2023, **33**, 2210656.
84. K. Zhang, J. Li, J. Zhang, S. Wang, X. Liu, T. Zou, H. Yang, X. Han and Y. Han, *Chem. Eng. Sci.*, 2025, **309**, 121461.
85. P. Mannu, R. K. Dharman, T. T. T. Nga, A. Mariappan, Y. C. Shao, H. Ishii, Y. C. Huang, A. Kandasami, T. H. Oh, W. C. Chou, C. L. Chen, J. L. Chen and C. L. Dong, *Small*, 2025, **21**, 2403744.
86. Y. Wang, G. Qian, Z. Xie, H. Yu, L. Li, J. Li, C. Chen, M. Lu and P. Tsiakaras, *Appl. Catal. B-Environ. Energy*, 2025, **365**, 124841.
87. X. Guo, Y. Li, Z. Xu, D. Liu, A. Kong and R. Liu, *Small*, 2025, **21**, 2408908.
88. M. Du, Y. Ji, Y. Li, S. Liu and J. Yan, *Adv. Funct. Mater.*, 2024, **34**, 2402776.
89. L. Liu, S. Li, Z. Zhang, C. Yin and Z. Yin, *J. Colloid Interface Sci.*, 2025, **696**, 137874.
90. J. Li, T. Gan, R. Yu, J. Cai, Z. Zhuang and H. Zhu, *Adv. Mater.*, 2026, **38**, e12893.
91. Y. Zhang, Y. Lei, Y. Yan, W. Cai, J. Huang, Y. Lai and Z. Lin, *Appl. Catal. B-Environ. Energy*, 2024, **353**, 124064.
92. R. Li, Y. Li, P. Yang, P. Ren, D. Wang, X. Lu, H. Zhang, Z. Zhang, P. Yan, J. Zhang, M. An, B. Wang, H. Liu and S. Dou, *Small*, 2023, **19**, 2302151.
93. J. Kim, M. C. Kim, S. S. Han and K. Cho, *Adv. Funct. Mater.*, 2024, **34**, 2315625.
94. Y. Liao, S. Deng, Y. Qing, H. Xu, C. Tian and Y. Wu, *J. Energy Chem.*, 2023, **76**, 566-575.
95. X. Yang, H. Zhang, B. Yu, Y. Liu, W. Xu and Z. Wu, *Energy Technol.*, 2022, **10**, 2101010.
96. N. Duan, T. Hou, W. Zheng, Y. Qu, P. Wang, J. Yang, Y. Yang, D. Wang, J. Chen and Q. Chen, *ACS Catal.*, 2024, **14**, 1384-1393.
97. A. Prajapati, C. Hahn, I. M. Weidinger, Y. Shi, Y. Lee, A. N. Alexandrova, D. Thompson, S. R. Bare, S. Chen, S. Yan and N. Kornienko, *Nat. Commun.*, 2025, **16**, 2593.
98. O. Moyo, J. Yang, J. Ding, Y. Zhang, J. He, J. Zhang and H. Sun, *Small Methods*, 2026, **10**, e02013.
99. Y. Lin, C. Deng, L. Wu, Y. Zhang, C. Chen, W. Ma and J. Zhao, *Energy Environ. Sci.*, 2020, **13**, 2602-2617.
100. H. Zhou, X. Duan, B. Huang, S. Zhong, C. Cheng, V. K. Sharma, S. Wang and B. Lai, *Angew. Chem. Int. Ed.*, 2025, **64**, e202422892.
101. J. Ge, J. Kuang, Y. Xiao, M. Guan and C. Yang, *Surf. Interfaces*, 2023, **41**, 103230.

No primary research results, software or code have been included and no new data were generated or analysed as part of this review.

View Article Online
DOI: 10.1039/D6CC01805J